UNIVERSITY OF CALIFORNIA, SAN DIEGO

Ultrafast X-ray Studies of Condensed Matter Systems in and out of Equilibrium

A dissertation submitted in partial satisfaction of the
requirements for the degree
Doctor of Philosophy

in

Materials Science and Engineering

by

James Wingert

Committee in charge:

Professor Oleg Shpyrko, Chair
Professor Prabhakar Bandaru
Professor Eric Fullerton
Professor Javier Garay
Professor Vitaliy Lomakin

2018

The dissertation of James Wingert is approved, and it is acceptable in quality and form for publication on microfilm and electronically:

_____

_____

_____

_____

_____

_____
Chair

University of California, San Diego

2018

DEDICATION

To Oleg, for giving me this opportunity; to my wife and family, for supporting me through it; to Andrej, for teaching me.

EPIGRAPH

You don't take a photograph, you make it.

— Ansel Adams

TABLE OF CONTENTS

LIST OF FIGURES

LIST OF TABLES

ACKNOWLEDGEMENTS

This work was supported by U.S. Department of Energy, Office of Science, Office of Basic Energy Sciences, under Contract DE-SC0001805.

Chapter 4 is, in full, is a reprint of the material as it appears in: J. Wingert, A. Singer, and O.G. Shpyrko. "A new method for studying sub-pulse dynamics at synchrotron sources." Journal of Synchrotron Radiation 22, no. 5 (2015): 1141-1146.. The dissertation author was the primary investigator and author of this paper.

Chapter 5 is, in full, is a reprint of a draft in preparation for submission: J. Wingert, A. Singer, S. K. K. Patel, R. Kukreja, M. Verstraete, A. Romero, V. Uhlíř, S. Festersen, D. Zhu, J. M. Glownia, H. T. Lemke, S. Nelson, M. Kozina, K. Rossnagel, B. M. Murphy, O. M. Magnussen, E. E. Fullerton, and O. G. Shpyrko "Direct time-domain determination of electron-phonon coupling strengths in Chromium." (To be submitted, working title.) The dissertation author was the primary investigator and author of this paper.

VITA

2006	Bachelor of Arts in Economics (*high honors*) and Physics, Oberlin College
2008	Master of Arts in Economics, University of California, Davis
2012	First Place, Sea Otter Classic Men's Pro Circuit Race
2013-2018	Research Assistant, Department of Physics, University of California, San Diego
2018	Doctor of Philosophy in Materials Science and Engineering, University of California, San Diego

PUBLICATIONS

J. Wingert, A. Singer, and O.G. Shpyrko. "A new method for studying sub-pulse dynamics at synchrotron sources." Journal of Synchrotron Radiation 22, no. 5 (2015): 1141-1146.

J. Wingert, A. Singer, S. K. K. Patel, R. Kukreja, M. Verstraete, A. Romero, V. Uhlíř, S. Festersen, D. Zhu, J. M. Glownia, H. T. Lemke, S. Nelson, M. Kozina, K. Rossnagel, M. Bauer, B. M. Murphy, O. M. Magnussen, E. E. Fullerton, and O. G. Shpyrko "Direct time-domain determination of electron-phonon coupling strengths in Chromium." (In preparation)

Singer, A., S. K. K. Patel, R. Kukreja, V. Uhlíř, **J. Wingert**, S. Festersen, D. Zhu et al. "Photoinduced enhancement of the charge density wave amplitude." Physical Review Letters 117, no. 5 (2016): 056401.

J. Carnis, W. Cha, **J. Wingert**, J. Kang, Z. Jiang, S. Song, M. Sikorski et al. "Demonstration of feasibility of X-ray free electron laser studies of dynamics of nanoparticles in entangled polymer melts." Scientific Reports 4 (2014).

Ulvestad, A., M. J. Welland, S. S. E. Collins, R. Harder, E. Maxey, **J. Wingert**, A. Singer et al. "Avalanching strain dynamics during the hydriding phase transformation in individual palladium nanoparticles." Nature Communications 6 (2015).

T. Saerbeck, J. Pereiro, J. Wampler, J. Stanley, **J. Wingert**, O.G. Shpyrko, and I.K. Schuller. "Ferromagnetism in partially oxidized CuCl." Journal of Magnetism and Magnetic Materials 346 (2013): 161-165.

S. Manna, J.W. Kim, M.V. Lubarda, **J. Wingert**, R. Harder, F. Spada, V. Lomakin, O.G. Shpyrko, and E.E. Fullerton. "Characterization of strain and its effects on ferromagnetic nickel nanocubes." AIP Advances (2017).

A. Singer, J.G. Ramirez, I. Valmianski, D. Cela, N. Hua, R. Kukreja, **J. Wingert**, O. Kovalchuk, J.M. Glownia, M. Sikiroski, M. Chollet, M. Holt, I.K. Schuller, and O.G. Shpyrko. "Non-equilibrium phase precursors during a photoexcited insulator-to-metal transition in V_2O_3." (In revision process with Physical Review Letters.)

ABSTRACT OF THE DISSERTATION

Ultrafast X-ray Studies of Condensed Matter Systems in and out of Equilibrium

by

James Wingert

Doctor of Philosophy in Materials Science and Engineering

University of California, San Diego, 2018

Professor Oleg Shpyrko, Chair

Over the last century or so, the diffraction of X-rays from periodic structures such as crystal lattices has yielded a vast number of breakthroughs in our understanding of condensed matter systems and how they are ordered. Over the course of this history, technical advances in the way X-rays are produced and measured have allowed for the structural characterization of solids to occur more and more rapidly. While clearly yielding an improvement in efficiency, the true scientific value of these advances is to allow determination of structural *changes* at shorter and shorter intervals. The capabilities of modern X-ray

sources are now becoming so advanced that it is possible to measure dynamics on the order of picoseconds, allowing scientists to measure "fundamental" phenomena not possible before, such as fast phase transformations and shockwaves. Dynamical studies of solids are naturally grouped into two categories: equilibrium, and non-equilibrium. This thesis is divided along the same lines. In the first part, a proposal is presented describing a new statistical method for studying equilibrium dynamics that could be implemented in the near future. In the second, experimental results showing the ultrafast propagation of an induced acoustic shockwave in a Chromium thin film are presented. This experiment was performed at the cutting-edge Linac Coherent Light Source (LCLS) at Stanford.

Chapter 1

A Very Brief Overview of X-ray Scattering and X-ray Sources

It is not my purpose here to provide an even remotely comprehensive exposition of x-ray scattering theory or a complete history of x-ray sources. Rather, I will briefly remind the reader why x-rays are important, highlight a couple important results from theory and discuss some features of modern x-ray sources that enable experiments such as those discussed in later chapters. A complete treatment of this subject matter can be found in many texts, both new [1] and old [2] [3].

"X-rays" are simply photons that have wavelengths which lie in a particular range of the electromagnetic spectrum. This range is roughly between a tenth of an Angstrom (10^{-10} m) and ten nanometers. This happens to be the lengthscale of atomic bond distances in solids, which is the reason for the profound importance of x-rays in the study of condensed matter systems. The discovery of this type of light is attributed to Wilhelm

Röntgen, for which he was awarded the first Nobel Prize in 1901. The discovery of x-rays owed to its high differential absorption in high-Z vs. low-Z materials. This can be used to cast shadows with an x-ray source on a chemical or electronic recording medium, a technique which still has profound importance in the medical profession. Physics, on the other hand, has benefitted largely from the diffraction effects that x-rays produce when they interact with the atoms in solid matter.

When x-rays are incident on the periodic structure known as a crystal, the light will scatter very intensely at certain special angles, forming a diffraction interference pattern in the far field. This effect was discovered by W.L. Bragg and W.H. Bragg (father and son) in the early 20th century, and was explained by them theoretically as well. The key insight was to consider a crystal, in a fixed orientation relative to some coordinate system, as a set of identical, repeating atomic planes. The planes obey Fresnel's law of reflection, so that light they reflect (emit) is at the same angle as the incident light relative to surface normal. When this angle is such that reflections from successive planes of atoms are out of phase by exactly one full cycle (or any integer multiple), constructive interference occurs. The now famous equation summarizing this simple two dimensional picture is known as Bragg's law: $n\lambda = 2dSin(\theta)$, where d is the spacing of the interatomic planes, θ the angle of incidence, λ the x-ray wavelength and n being a positive integer.

The pioneering work of the Braggs ushered in an entire field of study known as crystallography, using x-rays to characterize crystalline matter. Their first great achievement was to solve the crystal structure of table salt, NaCl, which has a cubic structure and a two atom basis. Later in the twentieth century, complex structures such as the DNA

double helix were solved. A complete description of x-ray scattering from solids combines two main ingredients: a mathematical formalism describing the positions of the electrons throughout the material/crystal, and a treatment of the (typically assumed to be elastic "Thomson") scattering of electromagnetic radiation from the individual electrons. There are multiple approaches to this, but the end result may be expressed as follows:

$$I(\vec{q}) = [\int_V \rho(\vec{r}) e^{-i\vec{q}\cdot\vec{r}} d\vec{r}]^2 \tag{1.1}$$

This elegant result may be expressed simply in words as well: the measured intensity at a point in reciprocal space ($\vec{q}$) in an x-ray diffraction experiment is given by the square of the Fourier transform of the electron density. The entire field of crystallography centers around characterizing the various regular structures found in nature that make up $\rho(\vec{r})$, and to characterize them mathematically in groups according to their symmetry. The work described in this thesis does not involve complicated crystal structures or experimental geometries, so I will not spend much more time on this subject. In fact, simply having knowledge of the two dimensional Bragg's law picture is probably sufficient to understand the scattering experiments and thought experiments I describe. Let me show a simple one dimensional example of this equation at work that qualitatively reproduces the diffraction pattern produced by the Chromium thin film described later in this thesis. In MATLAB, I define a 1-D perfect crystal of 100 atoms as follows (with a lattice spacing of 2.88 $\mathring{A}$):

>>a = 2.88;

>>N = 100;

```
>>r = a * (0:N-1);
```

I then create a reciprocal space vector of the appropriate range:

```
>>q = 4.36 + linspace(-.25,.25,1024);
```

Then we take the Fourier transform of our "lattice":

```
>>for m = 1:numel(q)
>>A(m) = sum(exp(-1j*q(m)*r));
end
```

Then we square this quantity and plot it in Q-space:

```
>>semilogy(q,abs(A).^2)
```

The result of this is shown in figure 1.1. The global maximum is this plot is known as a Bragg peak, the location of which is fixed by the width of the unit cell specified. The oscillations on either side of this maximum are known as Laue fringes, and their periodicity is determined by the width of the finite crystal.

I will now briefly discuss the history of x-ray production and detection, and where those technologies have now progressed, which is important to understanding this work. The first laboratory x-ray sources were what are often now referred to as "tube" sources. They are still widely used because of their simplicity and size. These devices consist of of a vacuum tube containing an anode and cathode separated by a large potential, across which electrons are accelerated. Upon crashing into the anode (typically composed of Tungsten or Copper), the electrons emit radiation in a broad range of energies as they are decelerated. This is known as *bremsstrahlung* or "braking radiation." On top of this broad

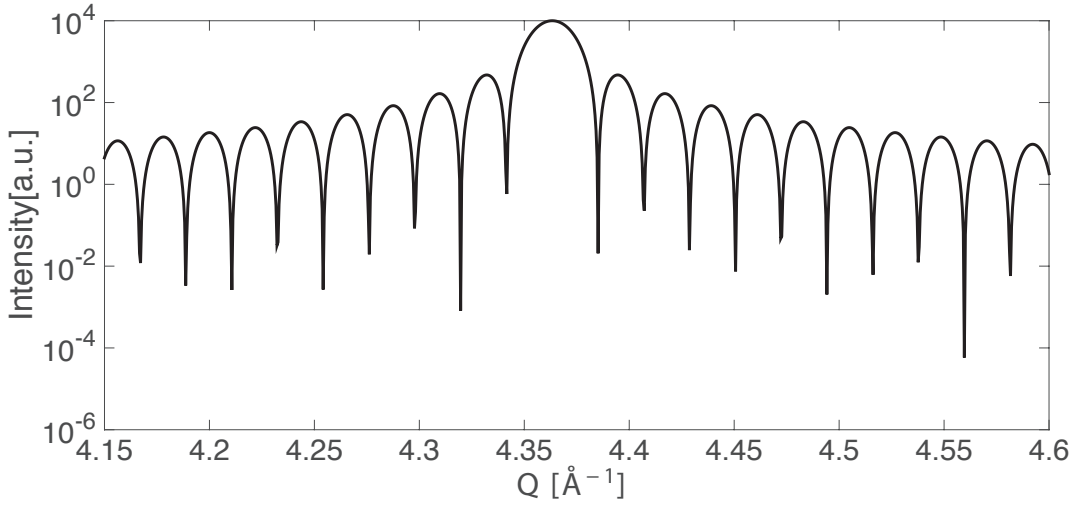

Figure 1.1: The simulated diffraction from a perfect one dimensional "crystal" that is 100 atoms thick, with a 2.88 $\mathring{A}$ "unit cell."

background, at two orders of magnitude higher intensity, are narrow emission "lines." These result when the incident electrons knock bound electrons in the inner shells of the atoms from their orbitals, whereafter less tightly bound electrons transition to the core shell, and a corresponding x-ray photon is emitted. This so-called characteristic radiation is typically the most desirable experimentally because of its well defined energy and high intensity. Monochromators are often used to isolate this radiation from the background in experiments. The most commonly used emission line is that corresponding to the K-edge of copper, having an energy of about 8000 eV.

The invention of the cyclotron and the synchrotron in the mid nineteenth century ushered in a revolution in x-ray science. Although they were created to be particle accelerators, the scientific community soon realized they were very useful sources of x-rays as well. At first, these x-rays were simply produced as a by-product of particle experiments

and used "parasitically" for diffraction experiments. Today, there are now many large storage rings created for the sole purpose of producing x-rays. In actuality, they are not truly rings, but rather many-sided polygons. Bending magnets curve the electrons paths into the straight sides, where they pass through so-called "insertion devices," which are periodic arrays of permanent magnets. This produces an x-ray beam with a very narrow energy spread and angular divergence. The intensity of the beam is also orders of magnitude brighter than what is possible from a tube source. The majority of cutting-edge x-ray experiments are performed at such facilities today. One important feature of storage rings is the time structure of the x-ray beam produced. Rather than being a continuous wave source like a tube, x-rays are emitted intermittently in short periodic bursts of about 100 picoseconds. This is because the electrons circling the ring are grouped together in bunches, because of the way they are accelerated and stored. This is quite important for what I discuss later in this thesis. Another important feature of these sources is that they produce partially coherent beams, so that some of the emitted photons are in phase with each other. This makes possible certain experiments that simply cannot be performed with a tube source, where each photon has a random phase with respect to the others.

In the last decade or so, a new technique for producing x-rays has been developed called a "free electron laser" (FEL). In actuality, it is not a laser, but it is capable of producing an almost fully coherent beam. It is similar to a synchrotron source in that it uses alternating permanent magnetic arrays to generate radiation, but it is built with a linear accelerator rather than a storage ring. The coherence properties owe to a process whereby the electrons interact with the photons they emit, becoming more and more or-

dered spatially and closer in phase. The pulses generated by such devices can be extremely short as well, down to tens of femtoseconds. This allows measurements with extraordinary temporal resolution to be made, such as those described later in this thesis.

The technology used in the detection of x-rays has closely mirrored that of visible light photography. The earliest methods were based on light sensitive chemistry (film). Today, as in medicine, two dimensional charge-coupled devices (CCDs) are the most common area detectors. As in action photography, the ability to make shorter exposures while still capturing enough light to make a serviceable image is of tremendous importance. Even today, the fastest x-ray cameras cannot be read out as fast as scientists would like to capture changes in diffraction patterns. Some of the work described in this thesis is aimed at using clever statistical techniques to make inferences about these changes in cases where detectors are indeed too slow to make sequential measurements. This work is inherently targeted toward capturing equilibrium fluctuations/changes in systems/diffraction patterns. The experiment presented in the final chapter of this thesis, on the other hand, involves non-equilibrium measurements, which are not limited by camera speed. In this case, a stroboscopic image making technique is used, much like how photographers exploit the shortness of light burts from flash bulbs compared to the speed of mechanical camera shutters. In our case, the flash bulb is a mutli-billion dollar free electron laser producing 50 femtosecond light bursts. The camera used to record them, on the other hand, operates at only 120Hz, more than 10 orders of magnitude slower.

Chapter 2

An Overview of Dynamic Light Scattering Techniques

The technique known as dynamic light scattering (DLS) is a technique that measures the time-dependent diffraction pattern created by coherent laser light incident on a moving sample to characterize the dynamics of the scatterers in that sample [4]. Here, a simple exposition of the quantitative methods involved are presented. Also, its application to critical opalescence of mixtures near their critical point is discussed. Finally, a technique known as speckle visibility spectroscopy (SVS) is discussed that is useful for studying systems with fast dynamics.

When coherent light is incident on a sample of non-uniform refractive index or thickness, an interference pattern is generated in the far-field that is known as *speckle* [5]. The speckle pattern from a perfectly static sample will be constant in time, aside from fluctuations due to noise. Figure 2.1 shows an example of speckle from a static sample

(scotch tape) produced in our laser lab. If, however, the scatterers themselves are in motion, then the speckle pattern will evolve in time. This connection between the sample and speckle dynamics can be made mathematically rigorous, so that much can be learned about the statistical properties of the motion of the scatterers.

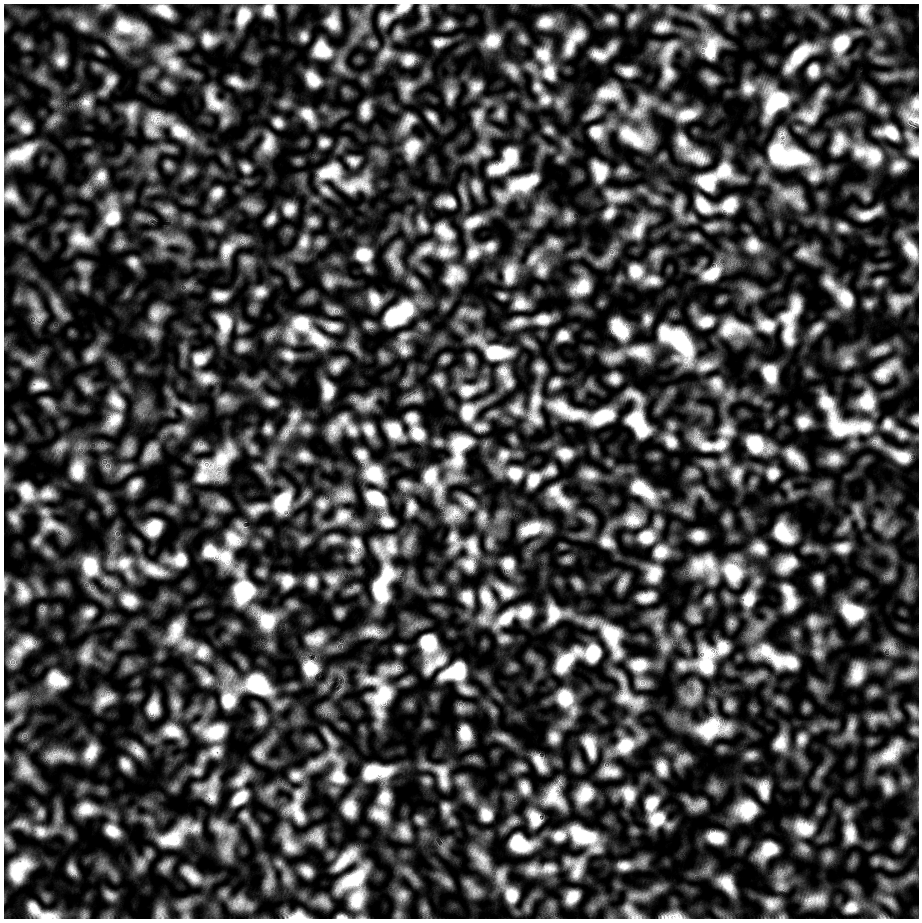

Figure 2.1: Speckle generated from scotch tape illuminated by laser light.

The simplest "textbook" scenario that can be presented is an ergodic system of mono-disperse (equal size/shape) particles that undergo Brownian motion. Many systems that can easily be prepared in a laboratory setting are well approximated by these assumptions. For example, a standard system used for calibrating a dynamic light scattering

(DLS) setup is a solution of polystyrene (PS) spheres, on the order of 100nm, suspended in glycerol.

In any photon correlation technique, such as DLS, which uses visible light, or x-ray photon correlation spectroscopy (XPCS), which uses x-rays, the quantity that is measured is the intensity of the scattered light in the far field. The intensities are measured with either a 2-D area detector, a 1-D "linescan" detector, or a 0-D "point" detector, and recorded as a function of time. This is done at some fixed angle of incidence, chosen appropriately for the system being studied. Whatever instrument is used, the time series of intensities measured is typically analyzed on a per-pixel basis and averaged, so it is sufficient to have in mind a one pixel point detector for the discussion that follows. As in many other fields where time series are important, the quantity of interest in photon correlation techniques is the (second-order) *autocorrelation function*:

$$g_2(\tau) = \frac{\langle I(t)I(t+\tau)\rangle_t}{\langle I(t)\rangle_t^2}. \tag{2.1}$$

Aside from the normalization factor in the denominator, this is simply the product of intensities at some fixed lag time, averaged over a sufficiently long time period. The first-order autocorrelation function, g_1, has the same form as the above, but is for the electric fields themselves:

$$g_1(\tau) = \frac{\langle E(t)E^*(t+\tau)\rangle_t}{\langle I(t)\rangle_t^2}. \tag{2.2}$$

Experimentalists begin by calculating g_2, since a photodetector measures intensities rather than fields. However, there is a frequently used and very important relationship

between these quantities, known as the *Siegert relation*:

$$g_2(\tau) = 1 + \beta|g_1|^2 \tag{2.3}$$

Ideally, one has $\beta = 1$, but in practice it is a parameter that is adjusted to fit the data and is less than unity. The statistical nature of the sample's dynamics will determine the specific shape of the autocorrelation functions. Regardless of this shape, however, in the limit as $\tau \to \infty$, g_2 will always decay to zero.

Let us now suppose that our sample is composed of spherical Brownian particles. In this case, each individual particle makes numerous small steps from its initial position that are independently distributed and numerous enough for the central limit theorem to apply. In such a situation, the probability that the particle has moved a distance r from its starting point is given by the Gaussian form

$$P(r) = (4\pi Dt)^{-3/2} e^{-r^2/4Dt}, \tag{2.4}$$

where D is the diffusion constant. In this special case, one can show that [6]

$$g_2(\tau) = 1 + \beta e^{-2Dq^2\tau}, \tag{2.5}$$

where q is the momentum or wave-vector transfer, which is the standard quantity that scatterers work with. It is completely determined by the angle of incidence of the beam on the sample and the energy of the incident light. Mathematically, it is given by

$$q = \frac{4\pi}{\lambda} Sin\frac{\theta}{2}. \tag{2.6}$$

Equation 2.5 is where the connection is made between what is measured experimentally and the properties of the scatterers themselves. By collecting data for several values of the parameter τ, a curve can be fitted to this simple exponential function, and D can be determined. Once D is known, if the experimenter knows either the viscosity of the fluid or size of the particles, the other can be inferred. This is typically done by exploiting the Einstein relation for self-diffusion [4]

$$D = \frac{k_B T}{\zeta}, \tag{2.7}$$

along with the Stokes approximation,

$$\zeta = 6\pi\eta a, \tag{2.8}$$

where η is the fluid viscosity and a is the particle radius.

DLS and XPCS would clearly be of limited utility if they could only be applied to monodisperse suspensions of spherical particles. In fact, the techniques are of great utility for a wide range of systems. Analytical extensions are possible for polydisperse systems (different particle sizes) and for non-spherical particles. Many complicated systems turn out to relax in a way that is described by a simple exponential decay. For example, figure 2.2 shows the autocorrelation function g_2 that was computed from data measured near the [400] Bragg peak of a lead crystal heated to near its melting point using coherent x-rays at the Advanced Photon Source.

Other systems that can be studied using DLS include those that exhibit critical opalescence [7], which occurs when a system approaches a second-order (continuous) phase transition. For example, many binary fluid mixtures will have a critical temperature at

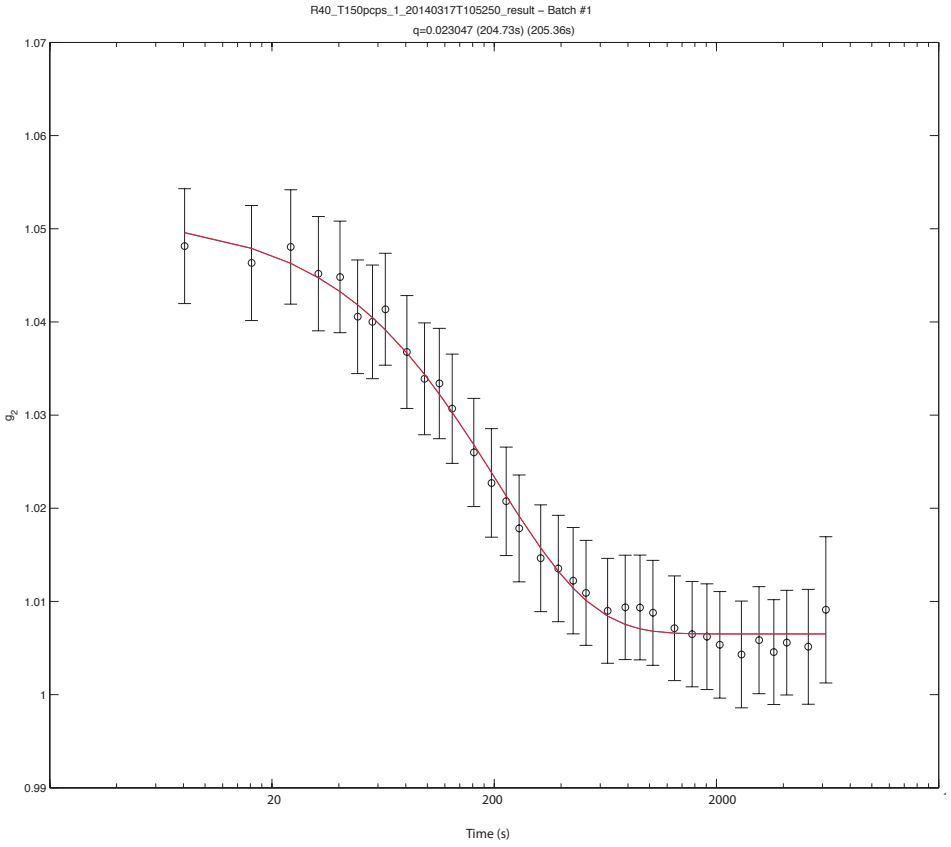

Figure 2.2: The autocorrelation function g_2 computed from data taken near the [400] Bragg peak of a single-crystal lead sample below its melting point.

which the equilibrium state switches from a one-phase state to a two-phase state. Single compounds also have a critical temperature separating the gas and liquid phases. At temperatures very near the critical point, where the free energies of the one and two phase states are equal, random thermal fluctuations will cause small volumes that are rich in one phase or the other to momentarily develop and then dissipate. The closer the system gets to the critical temperature, T_c, the larger the radius of the random volume fluctuations become. When these volumes exceed the wavelength of light (they can become *much* larger), the fluctuating refractive index in the sample gives rise to dynamic speckle, just

as the random motion of Brownian particles does. In fact, the mathematical form for the autocorrelation functions will be exactly the same as for the Brownian particles. The expressions involving the diffusion constant D still hold, and the theory is amended by replacing the particle radius with the characteristic size of the volume fluctuations.

As the critical temperature of a compound or binary mixture are approached, in addition to fluctuations in the speckle pattern, the total fraction of light scattered increases as well. This is observed as a pronounced cloudiness that develops at the critical point. Experimentally, it is measured as a sharp minimum in the intensity of light transmitted through the sample. Because this divergence is often so strong, and of narrow width around T_c, the fraction of light absorbed by the sample can be used as a sensitive probe to measure changes in T_c. For example, in [8], the effect of an applied electric field on the critical opalescence is studied. The field induces a change in the free energy associated with concentration fluctuations in a binary mixture, so that more work is required to create a fluctuation of a given volume in the presence of the field. (The way this arises is complicated mathematically, and is related to the non-linear curvature of the expression for the dielectric constant of the mixture of two fluids.)

In recent years, the extension of DLS techniques to x-ray wavelengths has allowed for the study of these fluctuations of binary fluids near their critical points at extremely short length scales, on the order of angstroms, as in ref. [9]. As they point out in that study, the binary fluids are in the same universality class as the 3-D Ising model, and an analytical connection between the scattered intensity of the light at various angles and the physical correlation length in the fluid can be made. (This connection occurs through the so-called

structure factor, $S(q)$, the fourier transform of which gives the scattered intensity.) The correlation length ξ is represented by a power law in the reduced temperature, $t = T/T_c - 1$, so that $\xi = \xi_0 t^{-\nu}$, and in the particular case of the hexane-nitrobenzene binary fluid studied, $\nu \approx 0.6$ and $\xi_0 \approx 3.5\mathring{A}$.

Many of the systems physicists are currently interested in do not relax in the simple exponential fashion. So-called "stretched" and "compressed" exponential forms are represented by [10]

$$g_2(\tau) = 1 + \beta e^{-\Gamma\tau^\alpha}, \tag{2.9}$$

where α is greater (compressed) or less (stretched) than unity. Also, "jammed" systems are of great interest in soft-matter physics currently. A jammed system will typically exhibit a two-step decay process. The first relaxation is due to diffusive motion by the scatterers, but it is incomplete because the scatterers are confined to diffuse within a local region of the sample, as often occurs in gels or glasses. The final long-term relaxation to $g_2 = 1$ only occurs when a large scale rearrangement of the system takes place. Because many particles rearrange at once when this happens, this final decay is very rapid when it does occur. Interestingly, many different systems exhibit a value of $\alpha = 1.5$ for the final decay [11].

Many physical processes occur on fast timescales such as picoseconds or even femtoseconds, but no existing detectors are able to be read out so rapidly. This means that the techniques described above cannot be implemented. There is, however, an alternative approach to measuring fast dynamics. It is based on studying the *contrast* of speckle

patterns.

What is typically meant by the "contrast" of an image is the standard deviation of the intensity, normalized by the mean. That is, $C = \sigma_I/\bar{I}$ [5]. Here, we will be working primarily with the square of this quantity, $V_2 = Var(I)/\bar{I}^2 = C^2$. These quantities are useful for analyzing speckle patterns in two ways. Firstly, they can be used to characterize the degree of beam coherence when the scatterers are static. Secondly, they can be used to analyze sample dynamics by quantifying the degree to which speckle patterns are"blurred out" when the scatterers are in motion.

Fully developed speckle results from large flux, perfect coherence, and a static scattering medium. In this speckle regime, contrast (and thereby V_2) should both equal unity. This is a result of the speckle intensities following an exponential distribution, for which the mean and variance are equal.[5] However, when the average number of photons per pixel (P) is small, V_2 can greatly exceed 1, and in fact diverges as $P \to 0$. Therefore, in the low-photon limit, it becomes impossible to detect either partial coherence or sample dynamics by measuring speckle contrast. This is due to the contribution of Poisson noise to the variance of the image. Formally, when static speckle from a beam possessing M coherent modes is overlaid with Poisson noise, the distribution of speckle intensity will have a Negative Binomial [M,P] distribution.[5] V_2 will then have an expected value of

$$< V_2 >= 1/M + 1/P. \tag{2.10}$$

In the technique known as speckle visibility spectroscopy (SVS), exposure times are

systematically varied to determine the resulting effect on speckle contrast. If shot noise is ignored, the following fundamental equation relates V_2 to the electric field autocorrelation function[12]:

$$V_2(T) = \frac{1}{\beta}[\frac{< I^2 >_T}{< I >^2} - 1] = \int_0^T 2(1 - t/T)[g_1(t)]^2 dt/T \tag{2.11}$$

The left-hand side of eq.3.2 is evaluated by recording multiple speckle patterns, with different exposure times. This can also be accomplished by computing the arithmetic mean of pixel values for a variable number of exposures/frames to create synthetic images with various effective exposure times (hereafter, "merging"). The right-hand side of (1) is evaluated either analytically or numerically after specifying a functional form for g_1. For example, choosing $g_1(\tau) = e^{-\Gamma t}$ will result in

$$V_2 = \beta \frac{e^{-2\Gamma t} - 1 + 2\Gamma t}{2(\Gamma t)^2} \tag{2.12}$$

This can be fitted to the measured values of V_2 to obtain an estimate of the parameter $\Gamma = \frac{1}{\tau}$. If multiple images, which are separated in time, are merged together to generate synthetic exposures, or if the light source is strobed (as it is for free electron laser (FEL) sources), the right hand side of eq.3.2 will need to be replaced by a discrete sum.

SVS techniques were originally developed using visible-light laser sources, where there are typically a sufficient number of photons to reduce the effects of shot noise drastically. However, when SVS is performed using an x-ray source (XSVS), shot noise will often have a considerable impact on contrast. Inoue *et. al.* [13] have recently been the first to demonstrate the feasibility of XSVS using a continuous-wave source (Spring-8)

with polystyrene spheres in glycerol by appropriately correcting for shot noise.

In the future, it is hoped that split-and-delay techniques will allow the $\sim$100 femtosecond x-ray pulses produced at FEL sources such as LCLS to arrive at the sample with arbitrarily short delay times, making it possible to probe dynamics on picosecond time scales. This will necessitate the use of SVS techniques, as no current detectors can be read out on picosecond timescales.[14]

Chapter 3

Contrast of Static and Fluctuating Speckle Patterns

3.1 Introduction

Analysis of the contrast (or variance) of speckle patterns is useful for many purposes. For example, the contrast of a speckle pattern produced by static scatterers indicates the degree of coherence of the illuminating beam. When dynamics are present, the dependence of speckle contrast on exposure time can be used to fit autocorrelation functions. This technique, known as speckle visibility spectroscopy (SVS), is particularly useful when detector readout speeds exceed the timescales of the system's dynamics. However, the analysis of speckle contrast is greatly complicated in the low-photon regime, where the contribution of Poisson (or "shot") noise dominates the signal. At a recent experiment at the Linac Coherent Light Source (LCLS) studying the dynamics of Polystyrene films [15],

we systematically varied the number of x-ray pulses hitting the sample during a single exposure, and analyzed the contrast of the resulting speckle. I show at what point it becomes possible to differentiate the genuine speckle from shot noise. Also, I show how the contrast analysis of a single frame can be used to identify sample damage. Finally, as a proof of principle, I show it is possible to fit autocorrelation functions directly from the time-dependent measurement of speckle variance.

What is typically meant by the "contrast" of an image is the standard deviation of the intensity, normalized by the mean. That is, $C = \sigma_I/\bar{I}$ [5]. Here, we will be working primarily with the square of this quantity, $V_2 = Var(I)/\bar{I}^2 = C^2$. These quantities are useful for analyzing speckle patterns in two ways. Firstly, they can be used to characterize the degree of beam coherence when the scatterers are static. Secondly, they can be used to analyze sample dynamics by quantifying the degree to which speckle patterns are"blurred out" when the scatterers are in motion.

Fully developed speckle results from large flux, perfect coherence, and a static scattering medium. In this speckle regime, contrast (and thereby V_2) should both equal unity. This is a result of the speckle intensities following an exponential distribution, for which the mean and variance are equal.[5] However, when the average number of photons per pixel (P) is small, V_2 can greatly exceed 1, and in fact diverges as $P \to 0$. Therefore, in the low-photon limit, it becomes impossible to detect either partial coherence or sample dynamics by measuring speckle contrast. This is due to the contribution of Poisson noise to the variance of the image. Formally, when static speckle from a beam possessing M coherent modes is overlaid with Poisson noise, the distribution of speckle intensity will

have a Negative Binomial [M,P] distribution.[5] V_2 will then have an expected value of

$$< V_2 >= 1/M + 1/P. \tag{3.1}$$

In the technique known as speckle visibility spectroscopy (SVS), exposure times are systematically varied to determine the resulting effect on speckle contrast. If shot noise is ignored, the following fundamental equation relates V_2 to the electric field autocorrelation function[12]:

$$V_2(T) = \frac{1}{\beta}[\frac{< I^2 >_T}{< I >^2} - 1] = \int_0^T 2(1 - t/T)[g_1(t)]^2 dt/T \tag{3.2}$$

The left-hand side of eq.3.2 is evaluated by recording multiple speckle patterns, with different exposure times. This can also be accomplished by computing the arithmetic mean of pixel values for a variable number of exposures/frames to create synthetic images with various effective exposure times (hereafter, "merging"). The right-hand side of (1) is evaluated either analytically or numerically after specifying a functional form for g_1. For example, choosing $g_1(\tau) = e^{-\Gamma t}$ will result in

$$V_2 = \beta \frac{e^{-2\Gamma t} - 1 + 2\Gamma t}{2(\Gamma t)^2} \tag{3.3}$$

This can be fitted to the measured values of V_2 to obtain an estimate of the parameter $\Gamma = \frac{1}{\tau}$. If multiple images, which are separated in time, are merged together to generate synthetic exposures, or if the light source is strobed (as it is for free electron laser (FEL) sources), the right hand side of eq.3.2 will need to be replaced by a discrete sum.

SVS techniques were originally developed using visible-light laser sources, where there are typically a sufficient number of photons to reduce the effects of shot noise drastically. However, when SVS is performed using an x-ray source (XSVS), shot noise will often have a considerable impact on contrast. Inoue *et. al.* [13] have recently been the first to demonstrate the feasibility of XSVS using a continuous-wave source (Spring-8) with polystyrene spheres in glycerol by appropriately correcting for shot noise.

In the future, it is hoped that split-and-delay techniques will allow the ∼100 femtosecond x-ray pulses produced at FEL sources such as LCLS to arrive at the sample with arbitrarily short delay times, making it possible to probe dynamics on picosecond time scales. This will necessitate the use of SVS techniques, as no current detectors can be read out on picosecond timescales.[14]

3.2 Some examples from LCLS data

At a recent experiment conducted at the XCS (X-ray Correlation Spectroscopy) beamline at LCLS (Linac Coherent Light Source), we studied the dynamics of polystyrene at temperatures approaching the melting point. Because split-and-delay techniques are not currently operational at LCLS, we worked with the standard 120 Hz repetition rate of the pulses for this experiment, which corresponds to a pulse separation of 8.3 ms. The number of pulses, N, that were scattered and recorded by a Princeton Instruments LCX CCD detector (1300 x 1300 pixels, 20 μm x 20 μm) before reading out could be varied. For one of the samples studied, the number of shots before readout was set to N = 2, 5, 10,

20, 50, and 100 to determine the effect this had on speckle contrast. The sample chosen consisted of gold nanoparticles (Au-NPs) of ∼10 nm in diameter embedded in polystyrene with a molecular weight of 42k (PS 42k), and held at a temperature of 170°C. The sample was studied in transmission at a photon energy of 8.7 keV, with the beam focused to a spot of approximately 3 μm. The sample to detector distance was chosen to be 685.8 mm, so that the speckle size at the detector would correspond as nearly as possible to the pixel size. For this sample, dynamics on the order of many seconds were anticpated, so for even the longest "exposure" in this set (∼800 ms), it was expected behave as an essentially static scatterer, assuming the beam was stable and sample damage did not occur. For the following analysis, unless otherwise noted, a small annulus of the image was used, centered at $Q = 0.034\mathring{A}^{-1}$, with a width of $\Delta Q = 0.1Q$.

At LCLS, the intensity of each individual pulse varies greatly, as can be seen in figure 3.1. In this particular run, only 2 x-ray pulses are recorded per frame, so the total intensity is very low. At such low intensities, almost all of the variation in V_2 is accounted for by these variations in intensity, and so it too will exhibit a similarly large variance. Figure 3.2 shows V_2 for the same data as figure 1.

Despite the very large variability in intensity and V_2, a log-log plot of V_2 vs. intensity for this data shows a clear linear trend with a slope of -1. This is shown in figure 3.3, plotted alongside $1/P$. At such low values of P, the contribution of the $1/M$ term is negligible, and the points should lie on the $1/P$ line. (See equation 3.1.) However, the points are uniformly offset from this line by roughly 1/4. This can be attributed to the spread of the electron cloud produced by individual photons across multiple pixels

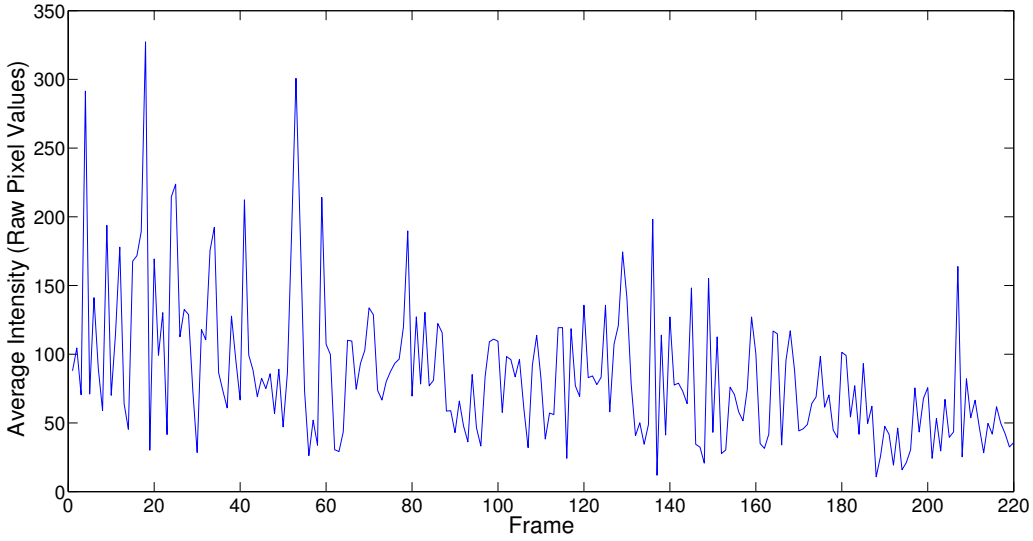

Figure 3.1: Frame-by-frame average intensity with 2 pulses hitting the sample per frame.

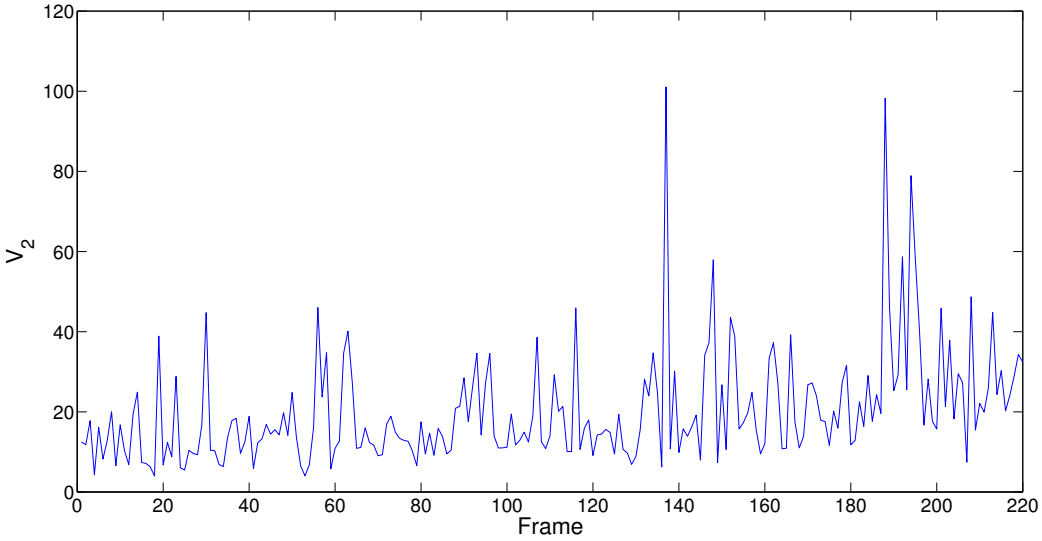

Figure 3.2: Frame-by-frame values of V_2 with 2 pulses hitting the sample per frame.

("bleeding"). Figure 3.4 shows a histogram of pixel values for all frames of a measurement of the same sample, with 10 pulses per frame. Since only 8.7 keV photons are detected, an 'ideal' detector would simply have a discrete distribution of point-masses located at integer multiples of the analog-digital-unit (adu). However, the ccd registers a continuous distribution of pixel values, with strong peaks at the adu value, approximately equal to 1650 here. This smearing-out of the ideal delta function peaks results in the data having a lower variance than a true Poisson distribution. To show that this indeed explains the discrepancy, we have binned the data into multiples of the adu[1] and repeated the same calculations. Figure 3.5 shows V_2 vs. intensity for the binned data, where the values now lie almost exactly on the predicted shot noise line. In demonstrating the feasibility of XSVS, [13] corrects for the effects of electron cloud bleeding by introducing a constant of proportionality $\epsilon/N, (0 < \epsilon < 1)$ for the shot noise contribution to V_2. The value of ϵ is determined by the relative sizes of the electron charge cloud generated by a photon and the pixel size. Our results are consistent with $\epsilon \approx 0.73$.

When the number of photons per pixel (P) is low, a log-log plot of V_2 vs. intensity will not show the influence of beam coherence or sample dynamics. In this limit, it is truly impossible to distinguish between genuine speckle and noise. However, as P increases, and the true speckle begins to emerge, V_2 will asymptotically approach the value $1/M$ from above. This can be seen when the data from the runs with varying numbers of shots per frame is plotted together, as in figure 3.6. Along with the raw data, curves are plotted for $1/M = 1$, $1/M = 0.05$, $1/M = 0.1$, and $1/M = 0.15$ These are labeled according to the

[1]Values between 0.5 adus and 1.5 adus are assigned to the adu value, etc.

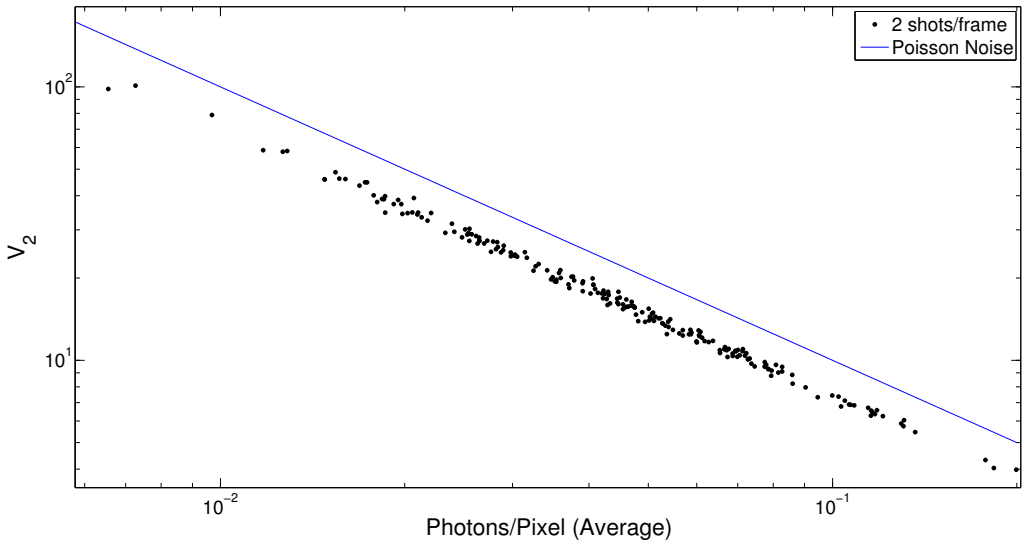

Figure 3.3: V_2 vs. average frame intensity with 2 pulses hitting the sample per frame.

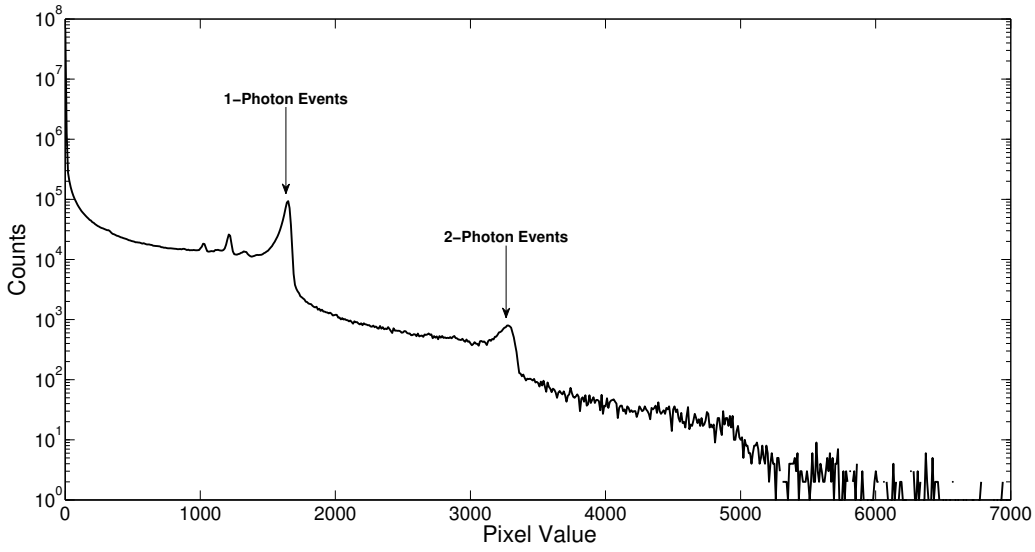

Figure 3.4: Histogram of pixel values for the run with 10 pulses recorded per frame. The full-frame images were used.

value of C that would result as $P \to \infty$, which we will call $C_\infty (= 1/M)$. To give a clearer view of the data for larger P values, a zoomed-in region of the graph is shown in figure

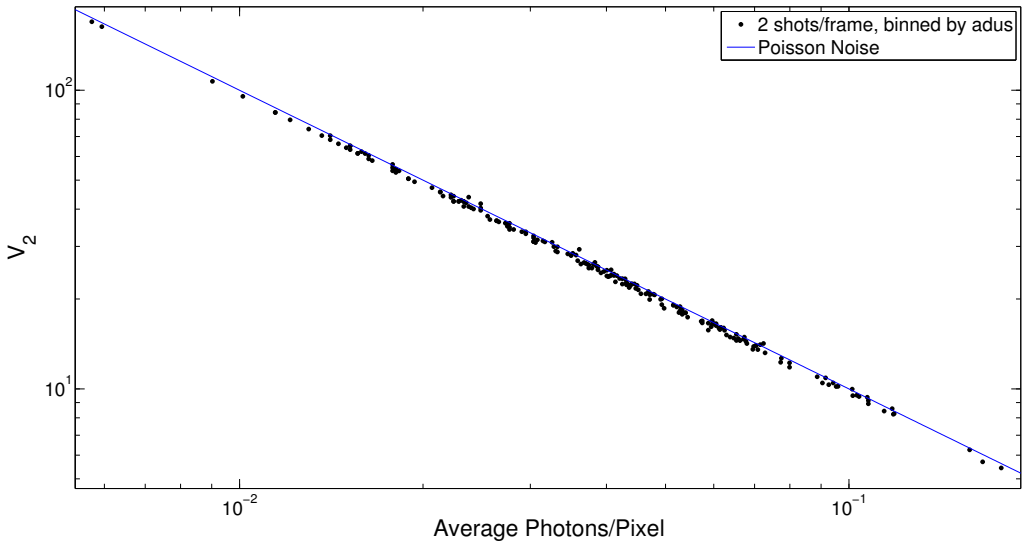

Figure 3.5: V_2 vs. average frame intensity for the binned data.

3.7. For each of the runs, the contrast of the speckle patterns appears to be consistent with a value of $C_\infty = 0.1$. As the LCLS source has perfect coherence for a single shot, this value seems surprisingly low. Sample damage and dynamics can both reduce contrast. However, both the $N = 50$ and $N = 100$ runs are consistent with $C_\infty = 0.1$, which would not be expected if sample dynamics/damage explained the reduction in contrast, because the $N = 100$ exposure is twice as long as the $N = 50$ exposure. Therefore the sample does indeed appear to behave as a static scatterer for the exposure times considered here. To illustrate this more clearly, figure 3.8 shows the same data alongside two data points that were generated by merging together many frames from the 5 shot per frame run. These points represent synthetic exposures of hundreds of seconds, which is presumably longer than the characteristic timescale of the dynamics. Therefore, only the component of contrast that is "static" is still present (approximately 5 percent). Beam "jitter" may

be a plausible explanation for the low contrast of the single frame exposures. However, our present purpose is simply to identify where the V_2 vs. intensity curve reveals the presence of real speckle. This clearly depends on the value of C_∞. If perfect coherence were preserved for multi-pulse exposures, speckle would become distinguishable just above $P = 0.1$, but with $C_\infty = 0.1$, this occurs closer to $P = 1$. This justifies our choice to use 50 pulses or greater per frame for the runs intended to study dynamics during this experiment.

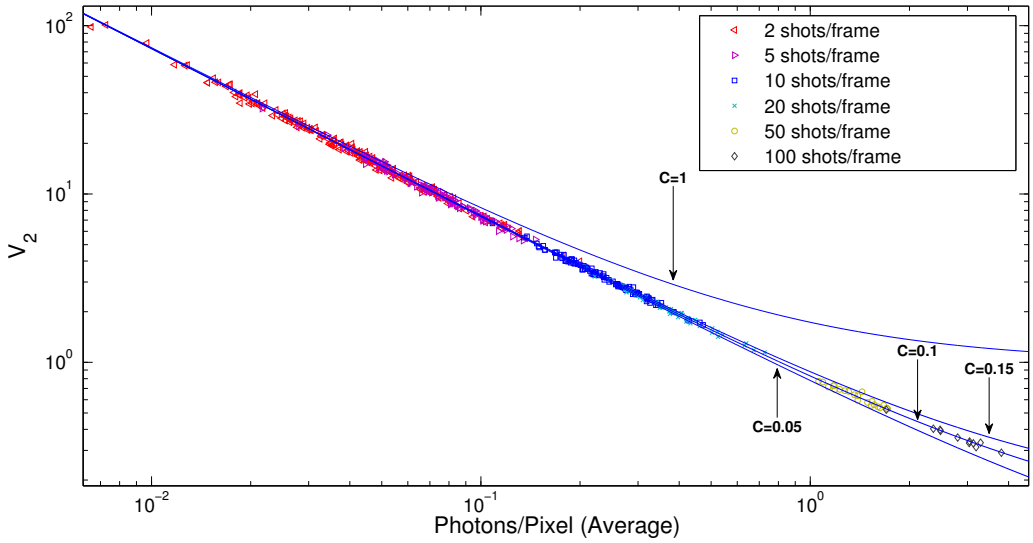

Figure 3.6: V2 vs. average photoevents/pixel, with curves shown corresponding to various values of contrast in the high photon limit.

Plots of V_2 vs. average intensity are also able to reveal sample damage. One of the samples we measured consisted of Au nano-rods in PS 1000k. This sample scattered much more strongly than the Au-NP samples. With 100 shots per frame incident on the sample, an order of magnitude more counts were detected than for the Au-NP sample previously discussed. Figure 3.9 shows V_2 vs. average intensity for this sample, along with the curve

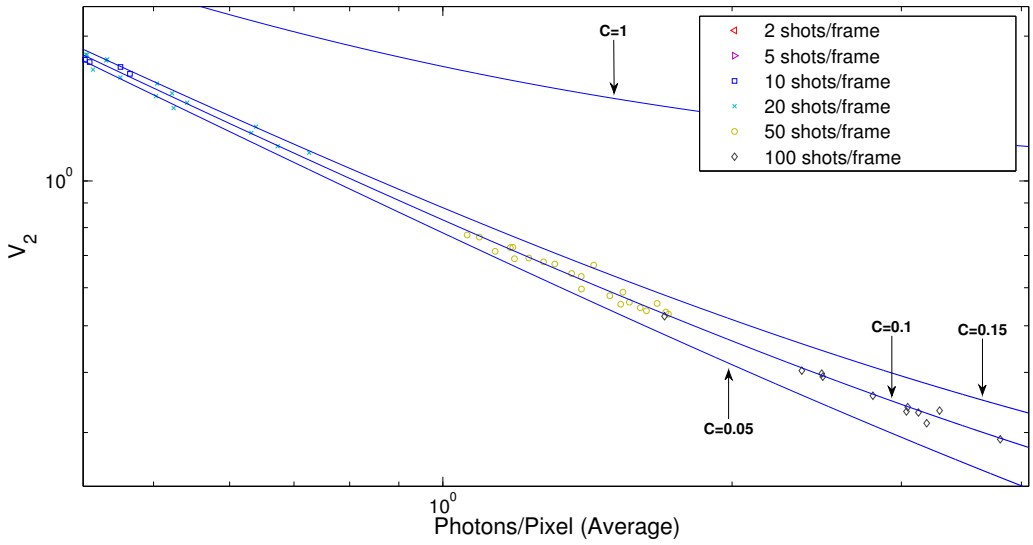

Figure 3.7: Zoomed-in view of a smaller region of the previous figure.

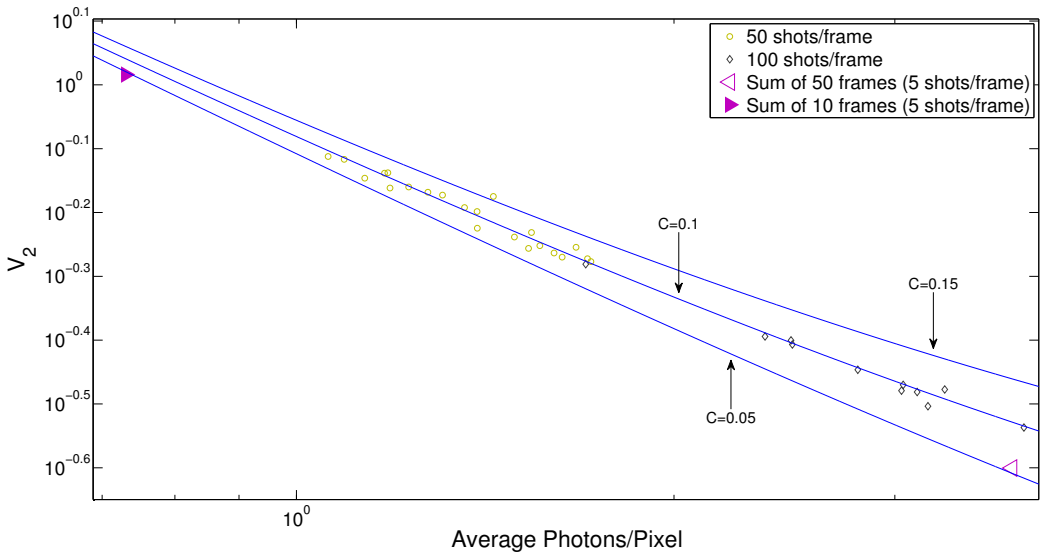

Figure 3.8: Zoomed view with data points included for many frames merged together.

$0.1 + 1/P$ that best fit the Au-NP visibility data. Instead of asymptotically approaching 10 percent, the contrast falls abruptly at higher intensities. Since all of the data points correspond to exposures of equal length, this intensity dependence of V_2 is evidence of the

beam heating or damaging the sample. Because plots of this type are easy to generate, they are a potentially useful way to determine quickly whether the flux per frame is both adequate to produce good signal noise and below the radiation damage threshold.

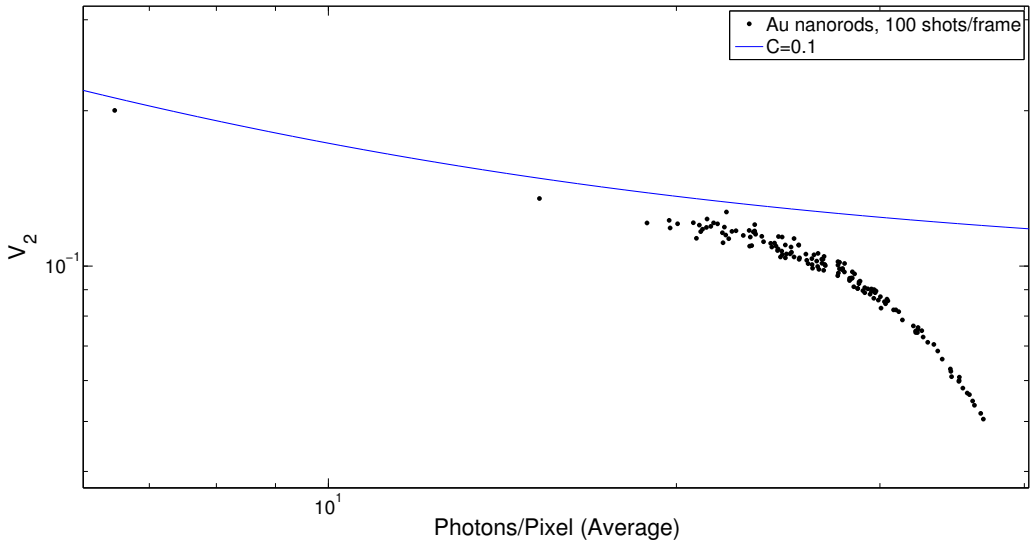

Figure 3.9: V_2 vs. average frame intensity for the Au nano-rods in PS 1000k at 120°C with 100 shots/frame. The sharp drop-off at higher intensities is indicative of sample damage.

To demonstrate the feasibility of the SVS technique with a pulsed FEL source, we also examined the contrast of synthetic images formed by merging together multiple frames. Figure 3.10 shows V_2 vs. frames merged for speckle patterns recorded with 100 pulses per frame incident on a PS 42k sample containing Au-NPs at a temperature of 120°C. The shot noise contribution to the variance has been subtracted. To produce an approximate fit to the data, a simple exponential distribution was assumed for the electric field autocorrelation function, and a discrete analog of eq.3.2 was used. Additionally, a static component of V_2 was included in the fit, so that $V_2 = \alpha + \beta V_2(T)$.

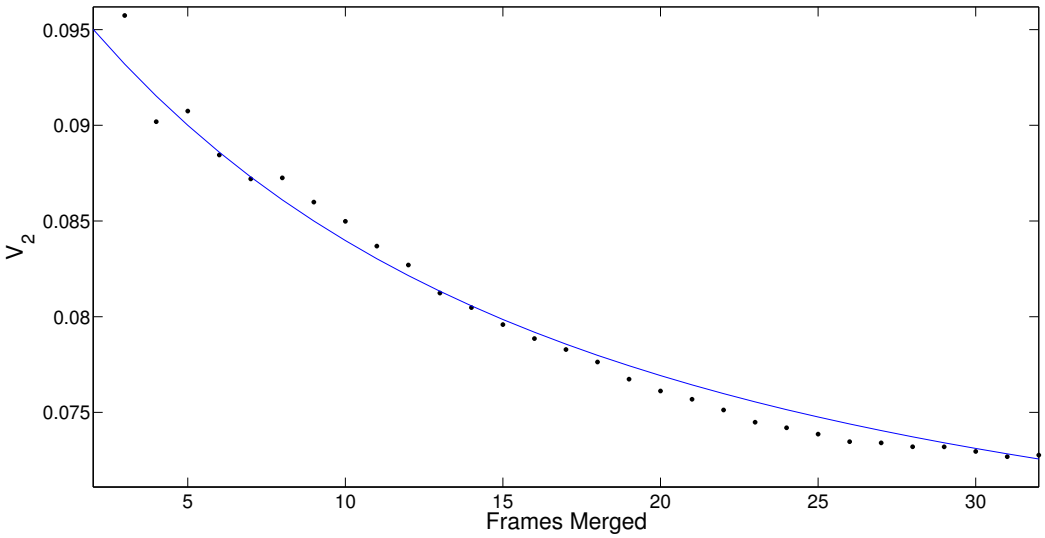

Figure 3.10: V_2 vs. frames merged for Au NP sample at 120°C with 100 pulses/frame. $\beta = 0.035$, $\alpha = 0.062$, and $\tau = 75$ were chosen to qualitatively best fit the data.

Chapter 4

A New Method for Studying Sub-Pulse Dynamics at Synchrotron Sources

4.1 Introduction

We investigate the possibility of studying dynamics on time-scales on the order of the pulse duration (∼100 ps) at synchrotron x-ray sources with present avalanche photodiode point detection technology, and without adopting pump-probe techniques. We find that sample dynamics can be characterized by counting single and double photon events and an analytical approach is developed to estimate the time required for a statistically significant measurement to be made. We indicate the amount of scattering required to make such a measurement possible within a few days, and show that at next generation

synchrotron sources this time would be reduced dramatically – by more than 3 orders of magnitude. We confirm our analytical results with simulations in the frame of Gaussian statistics. We forsee that in the future our approach can be extended to even shorter time-scales with the implementation of ultrafast streak cameras.

Studying fast dynamics with x-rays is of ultimate importance in many areas of research including chemistry [16], condensed matter physics [17] and atomic physics [18]. The recent development of new generation x-ray sources allows for the combination of atomic resolution due to x-ray wavelengths and fast time-scales due to the pulsed nature of these sources. Conventional x-ray photon correlation spectroscopy (XPCS) measurements rely on correlating sequential intensity measurements. For this reason, the time separating the individual pulses of the source (on the order of 100 ns) is often viewed as a lower limit on the time-scales that can be measured. Pump-probe experiments at storage ring sources are inherently limited by the pulse duration, about 100 ps, and suffer from the low repetition rate of pump laser systems. To go beyond this limit, slicing techniques are applied with an increase of temporal resolution by two orders of magnitude, however, at a significant expense of photon flux [19]. The development of x-ray free-electron lasers (XFELs) [20, 21, 22, 23] with ultrashort pulse durations (10-100 fs) has led to an improvement in time resolution by about three orders of magnitude. However, today XFELs suffer from intrinsic fluctuations and are still rare and highly overbooked. Here we propose an alternative method, i.e. by utilizing coherent x-ray scattering to enhance the time resolution at synchrotron sources and go below the pulse duration without sacrificing flux.

Coherent x-ray radiation is a superb probe for studying dynamics on the atomic

scale. In a typical XPCS experiment, speckle is observed due to interference [24] and small changes of the sample can be tracked using intensity correlation techniques. Dynamics for times ranging from fractions of a microsecond to hours [25, 26, 27] have been studied using XPCS. However, similar to intensity interferometry experiments [28] at synchrotron sources, the time resolution is limited by the pulse duration of the source [29]. This is significantly shorter than the time-scales that can be observed using conventional XPCS, with which it is not possible to study time-scales shorter than the inter-pulse separation. Synchrotrons are nowadays the principle sources of high-brilliance x-ray beams and we anticipate that our technique can extend the application of these sources to the sub-100 ps time regime, without using pump-probe methods. At present, only pump-probe experiments are able to access time-scales shorter than the pulse separation, but these are inherently out-of-equilibrium studies.

Studying dynamics at time-scales on the order of the pulse duration at synchrotron sources will necessitate working in a low photon regime. In the very low photon limit, the basis for assessing the dynamics within a sample will naturally be cast in terms of the relative frequency of single and double photon events measured at a detector. Single and double photon events can be counted using an avalanche photodiode (APD) point detector [30]. Such a device can be read out rapidly, so that a separate measurement is possible for each synchrotron pulse. For synchrotron x-ray intensities, the vast majority of the recorded intensities will be dark noise, along with some rare single photon events. Also, very rarely, an intensity corresponding to two photons from the same pulse will be recorded. We will call such an event a "double," while measurements registering a single

photon will be called "singles," and those with a dark noise value "zeros." Figure 4.1(a) depicts these three possibilities.

Recently, the feasibility of making XPCS measurements within the time-scale of a single synchrotron pulse has been considered by employing a "streak camera" [31, 32, 33]. Simplistically, such a device "sweeps" the signal along a column of pixels over the duration of a single pulse so that the vertical direction represents time (see Figure 4.1 (b)). Unlike the point-detector approach, this allows the time separating individual photons that arrive in a single pulse to be identified. This can be done with an area detector as well so that multiple measurements are made simultaneously. To be attractive, such a device would need to be read out at the ring repetition rate of present synchrotron sources (often about 6.5 MHz), which may prove the most difficult aspect of its implementation. However, it should be noted that this might be made less challenging by the extremely sparse nature of the data, which may lend itself to reduction by some appropriate hardware.

The approach we develop for studying sub-pulse dynamics does not require the implementation of the streak camera concept, although it is a very exciting prospect that we discuss. We show that sample dynamics can still be studied without resolving the temporal separation of the two photons that comprise the doubles, and this is our most important result. Existing APD point-detectors are the best candidate for the first measurements to implement our approach. By varying the time-scale (τ) of the dynamics of interest, for instance by changing the temperature, one could establish a crossover point for the type of relaxation being studied. The signature of the crossover will be a transition in the relative frequency of the doubles.

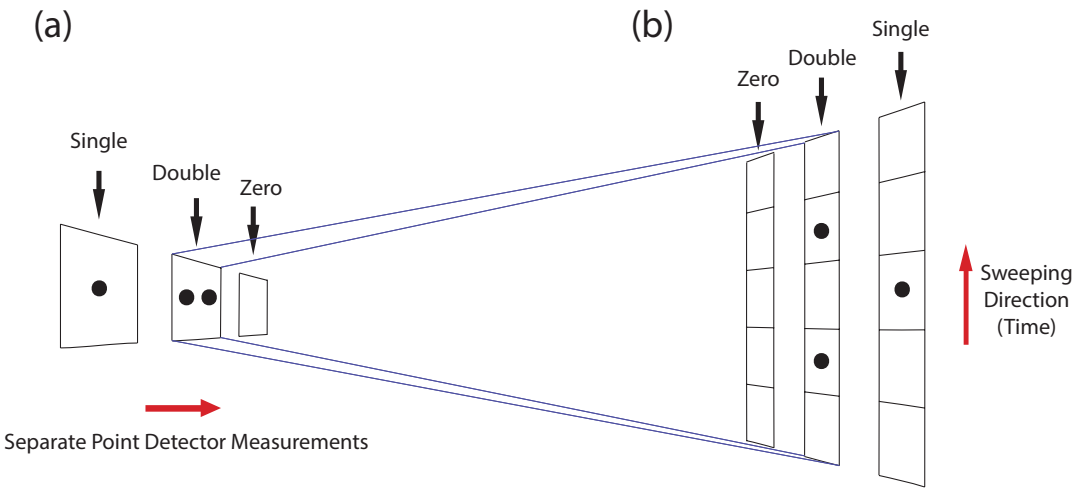

Figure 4.1: Two approaches to studying intrapulse dynamics. (a) depicts separate measurements made with a simple point detector, and three possible outcomes. (b) shows the streak-camera approach to the same measurements. A single point detector measurement is equivalent to integrating the counts on the streak camera.

Because the APD technique does not depend on correlating individual intensity measurements in time, it becomes possible to go below the "fundamental" limit of roughly 100 ns imposed by the pulse frequency all the way into the 100 ps regime. This is an impressive 3 order of magnitude improvement in the measurable time-scale. However, because all of the photons are concentrated into short pulses, no extra flux is required to make a measurement with comparable signal-to-noise as the case where intensities from sequential pulses are being correlated. The proposed technique fully utilizes the capabilities of synchrotron sources.

The feasibility of studying dynamics that occur within a single pulse has already been demonstrated at XFEL sources [14, 34]. The much larger coherent flux from such sources results in multiple photons frequently being counted per pixel. Our method is very

similar conceptually, but our analysis differs as a result of the lower flux from synchrotrons, which necessitates that we only consider one and two photon events.

4.2 Estimating Number of Measurements and Time Required

We reduce the correlation analysis applied in XPCS to counting single and double photon events. The statistical distribution that generates the speckle will determine how rare the doubles are relative to the singles, and will form the basis of our analysis. Our goal here is to estimate the minimum amount of time required in order to draw statistically significant conclusions about the presence of dynamics in a sample of interest. To do so, we perform some straightforward statistical calculations comparing the relative frequency of doubles to singles for two extreme cases: speckle from a sample with dynamics significantly slower, and much faster, than the pulse length. In these extreme cases, the spacing of the two photons that make up the double is irrelevant (all spacings are equally probable), so it is best to have in mind point-detector measurements for the following.

We begin our analysis by presenting the distributions corresponding to the two extreme cases. A quasi-static sample (static on the time-scale of the pulse) will generate a persistent speckle pattern, as in figure 4.2(a), whereas a highly dynamic sample will produce a speckle pattern that is "washed out," as in figure 4.2(b). For speckle generated by a quasi-static sample, illuminated by a beam with r transverse coherent modes and scattering an average of m photons per speckle, the probability of k photo events per

speckle is given by the negative binomial distribution [5]:

$$P_S(X = k) = \left(\frac{r}{m+r}\right)^r \frac{\Gamma(k+r)}{k!\Gamma(r)} \left(\frac{m}{m+r}\right)^k, \tag{4.1}$$

where $\Gamma(k)$ is the gamma function. The negative binomial distribution applies to the intensity distribution of *each point in a single speckle pattern*. However, it will also describe the distribution in time for *one individual speckle in that pattern* if the entire pattern varies on time-scales (even many decades) longer than the pulse duration. This will clearly be the case for any system being investigated in the ultrafast regime. It would also be true for a *completely* static sample if either the sample or detector were translated occasionally.

For x-rays scattered by a sample that de-correlates much faster than the duration of a pulse, there will no longer be genuine speckle, and the distribution of intensities will simply be given by the well-known Poisson distribution:

$$P_D(X = k) = \frac{e^{-m} m^k}{k!} \tag{4.2}$$

The ratio of doubles to singles forms the basis of our analysis, as it allows one to determine whether some given data is generated by one distribution or the other. The probability of a double, in the quasi-static case, is $P_S(X = 2)$, given by equation (4.1). If τ is the time-scale of the physical process of interest, then in the $\tau \to 0$ limit (the "dynamic" sample), the probability of a double will be $P_D(X = 2)$, according to equation (4.2). In both cases, the number of doubles will be binomially distributed [35], with the

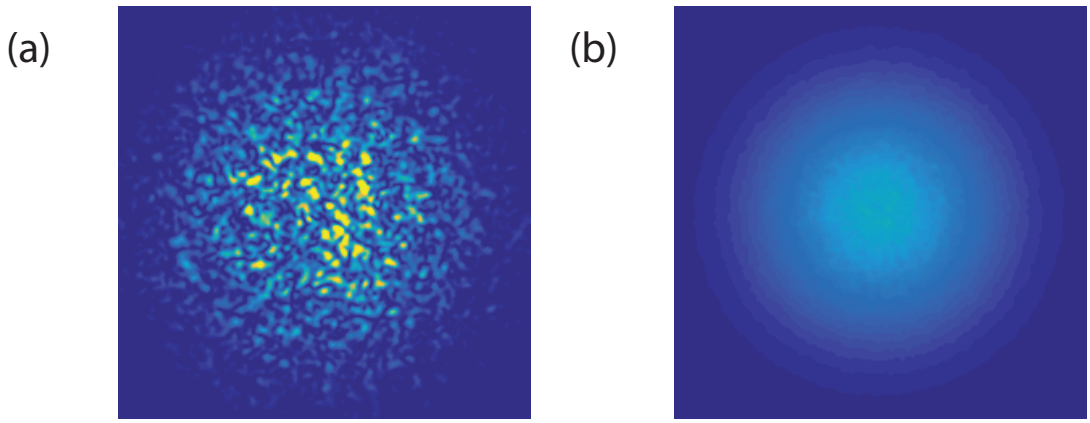

Figure 4.2: (a) A simulated speckle pattern from a quasi-static sample. (b) The average of 1000 such random speckle patterns, representing a dynamic sample.

expected number of doubles given by $\mu_j = NP_j(X = 2)$, and a variance of $\sigma_j = NP_j(X = 2)[1 - P_j(X = 2)]$ around this value, where j is D or S. In the low-photon limit, both distributions have an expected number of singles equal to Nm. [1]

We now want to calculate how many individual measurements need to be made to discriminate between data coming from the quasi-static and dynamic samples for a given set of parameters. To do so, we suppose that our sample is in fact quasi-static (our null hypothesis), and ask how long one must measure in order to rule out the $\tau \to 0$ case at a statistically significant level. A standard t-test[35] for this null hypothesis would then compute $t = (Y - \mu_D)/\sigma_D$, where Y is the actual number of doubles collected. The expected value of this quantity, if the sample is truly quasi-static, will be

[1] In principle, one could consider number of triples, etc., but in the low-photon limit considered here these will almost never occur.

$$E(t) = \frac{\mu_S - \mu_D}{\sigma_D}. \tag{4.3}$$

Using equation (4.3), we calculate the number of measurements N required to discriminate between a quasi-static and dynamic sample. We choose to use a 3σ confidence level for the calculation. Figure 4.3 shows a plot of the value of N that solves $E(t) = 3$ for different numbers of modes r on a log-log scale. The linear shape of the curve at low m indicates an inverse-square dependence. In fact, it can be shown by a straightforward calculation that for $m \ll 1$, the solution to equation (4.3) can be approximated by

$$N \approx \frac{18}{m^2(r^2 + r - 1)^2}. \tag{4.4}$$

Notice that there is a minimum in N for each of the curves, which occurs at about $m = 0.19$ for the $r = 1$ case. The reason for the minimum is that as m increases beyond this value, the probability of a double for the Poisson distribution approaches that of the negative binomial. The probability of a double becomes *more* likely with Poisson statistics when m reaches about 0.47, for the $r = 1$ case. (See figure 4.3.)

To estimate actual measurement times for a realistic example we consider the Advanced Photon Source (APS), which is a state of the art synchrotron source. In our calculation we assume full coherence, so that $r = 1$. We then estimate the coherent flux, m, and compute the time required to discriminate between quasi-static and dynamic systems for four situations, which are summarized in Table 4.1. The first case corresponds to an approximation for a generic experiment performed at APS with current operating

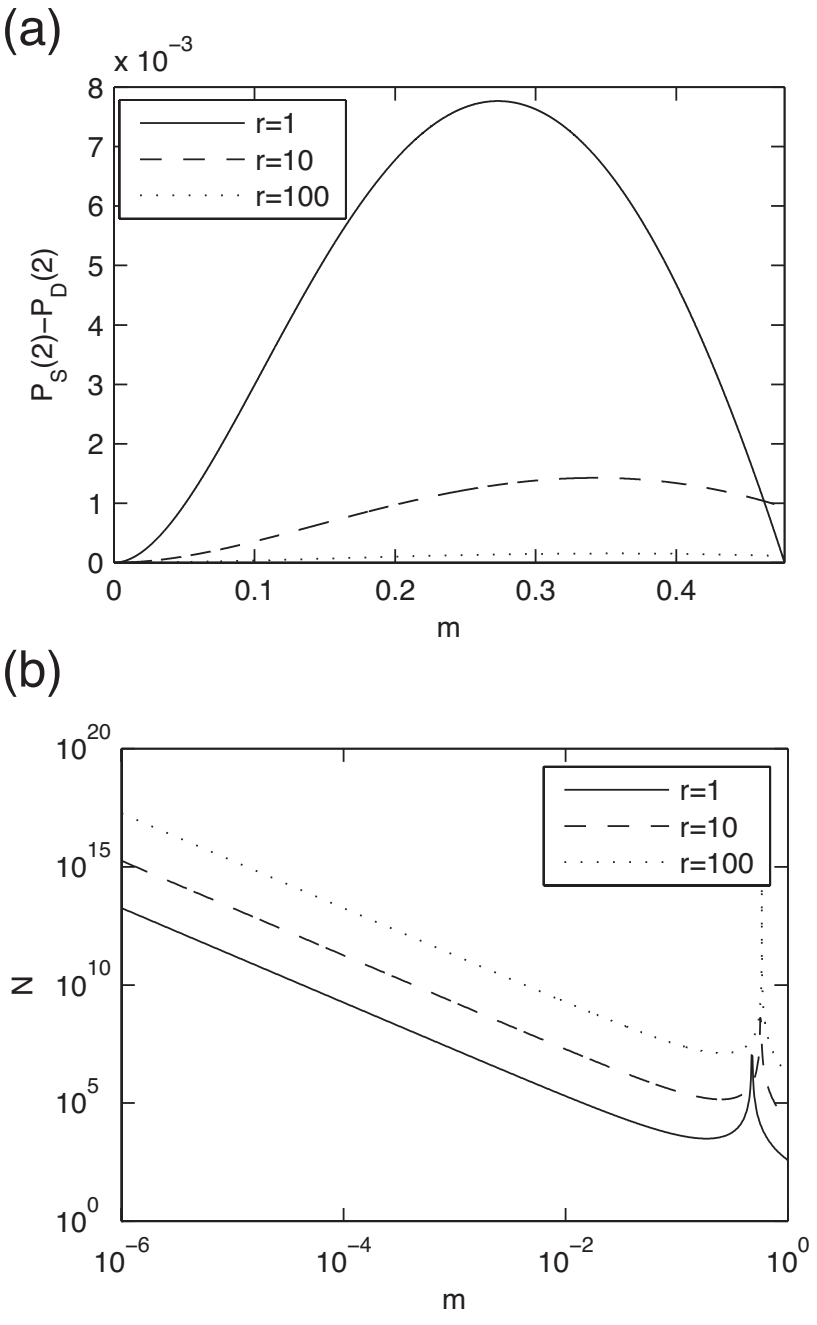

Figure 4.3: (a) The difference in the probability of a double for the two distributions. (b) The expected number of measurements, N, which must be collected for a 3σ result.

parameters. We consider optimized experimental geometry with the speckle size being matched to one pixel [36] and m is calculated by assuming 10 photons scattered into our point-detector (or each speckle) per second. Whether this amount of scattering can be achieved in a geometry that is suitable for measuring length-scales that corresponding to the time-scales in question can be determined by the experimentalist. However, this level of scattering represents an important cutoff, as it results in the measurement being achievable on the order of several days, which is the length of a typical beam-time. The second situation would correspond to 10^9 photons/s of coherent flux and a fraction of 10^{-4} of the direct beam being scattered into the detector.[2] The third and fourth scenarios are the same as the first two, but are estimated for the proposed APS upgrade, where coherent flux is expected to be about 2 orders of magnitude higher. In all cases, if the sample in indeed quasi-static, and one collects the number of pixel values listed in Table 4.1, the expected total number of doubles is about 20, compared to about 10 in the Poisson case.

It is worth discussing how the measurement times computed here change if we do not assume full coherence. This is a practically important question, because present synchrotrons are not currently fully coherent sources. It is possible, however, to apply spatial filtering to reduce the number of coherent modes at the expense of flux. Our calculations show that, if one is in a linear regime where modes and flux can be scaled by the same factor,[3] it is always preferable to have fewer coherent modes. However, for low values of m, such as those listed as "typical" experimental values here, there is almost no

[2]This second situation is not intended to represent an achievable scattering cross-section for a realistic experiment, but rather to set a sort of lower bound on the measurement time for comparison.

[3]So that one could choose between 10 photons/second and one coherent mode or 100 photons/second and 10 modes.

change ($< 0.3\%$) in measurement time. For the values of m corresponding to partial direct beam, measurement times could be reduced by more than a factor of two for spatially filtered beams. Importantly, spatially filtering becomes less effective in the high coherence regime[37] and an optimization of the experimental parameters will be required in this case.

4.3 Numerical Simulations

To confirm our analytical findings we perform simulations in the frame of Gaussian statistics [5]. In particular we simulate an ensemble of scatterers, whose dynamics can be represented by a predefined time-scale. If we illuminate such a system with coherent x-rays and the typical geometrical conditions for XPCS are met [36], the time dynamics can be studied by intensity evolution of the speckle. For simplicity, we consider only a single momentum transfer vector and assume the evolution of the speckle behaves according to Gaussian statistics. This can be simulated using a model presented in [38]. The starting point of the model is a signal in time with constant amplitudes and completely randomized phases. To induce correlations in time, one can apply filtering in the Fourier space, i.e. the signal is Fourier transformed, multiplied by a filter function, which is a Fourier transform of the desired autocorrelation function in time, and Fourier transformed back. To obtain a negative exponential autocorrelation function of the form $e^{-\alpha t}$, which is typical for diffusive dynamics with a time constant $\tau = 1/\alpha$ and is found in many systems,[4] we use a filter function of the form $1/(\alpha + i\omega)$, where ω is the frequency. By modifying the width

(τ) of the autocorrelation function, we are able to define the time scale of the system. Figure 4.4 shows the simulated time evolution of a speckle for the case of $\tau = 10$ ps time dynamics, if we interpret each data point as corresponding to 1 ps. The width of the "spikes" corresponds to the aforementioned time scale. Note that for the limiting case of fast dynamics, this intensity profile is simply replaced with a flat line.

In the point-detector approach to studying dynamics, it is not possible to measure directly the spacing between photoevents within the sample; it is only possible to say how many photons were incident on the detector per pulse. But by varying a physical parameter related to τ, such as the temperature, the time-scale of the dynamics can still be studied. This can be demonstrated by varying the "spike" width in our simulations. Figure 4.5(a) shows the relative probability of a double vs. τ for different numbers of measurements. For this figure, and the other simulation results shown here, we have chosen $m = 0.01$. As the number of measurements increases, it becomes possible to see the transition from the dynamic to the quasi-static regime. This occurs at about $N = 10^6$ for the simulations shown, which is consistent with our analytical calculations. In future experiments of this nature, given a sufficient quantity of data, it will be possible to estimate relaxation times using this analysis.

If the data instead comes from a streak camera device, with time resolution better than the pulse duration, it will be possible to measure directly the spacing of photoevents that make up our doubles, and traditional XPCS methods become possible. This is equivalent to interpreting the data shown in figure 4.4 as a single pulse (which would be a double in this case), rather than a sequence of separate APD measurements (in which case

it would count as two singles). In XPCS, the quantity of interest is

$$g_2(\tau) = \frac{\langle I(t)I(t+\tau)\rangle_t}{\langle I(t)\rangle_t^2}, \tag{4.5}$$

where $I(t)$ is the intensity measured at time t and τ is the time delay. Typically, g_2 has its maximum value for zero time delay and the width of the function represents the time scale of the dynamics of the system. In the extremely low photon regime we consider here, the numerator will take on values of 0 or 1 almost exclusively, since nearly all pixel values are either 0 or 1. In this case, g_2 simply becomes the probability of a double at fixed τ plus one, and should therefore reduce to a simple (normalized) histogram of the number of doubles vs. separation time, τ. Any small difference between the histogram values and the g_2 function arise from the presence of a few pixels with a value greater than 1. Figure 4.5(b) shows a comparison of equation 4.5 with the histogram approach for the simulations for $\tau = 10$ ps. That the histogram approach is essentially equivalent to traditional XPCS methods in the low photon regime may prove important, as it potentially allows for the reduction of very large sets of data.

4.4 Conclusion

In conclusion, our analytical findings and numerical simulations show that the analysis of sample dynamics shorter than a synchrotron pulse duration is possible using current technology. The analysis of sample dynamics in such a regime consists of the study of the relative frequency of single and double photoevents. We forsee that with

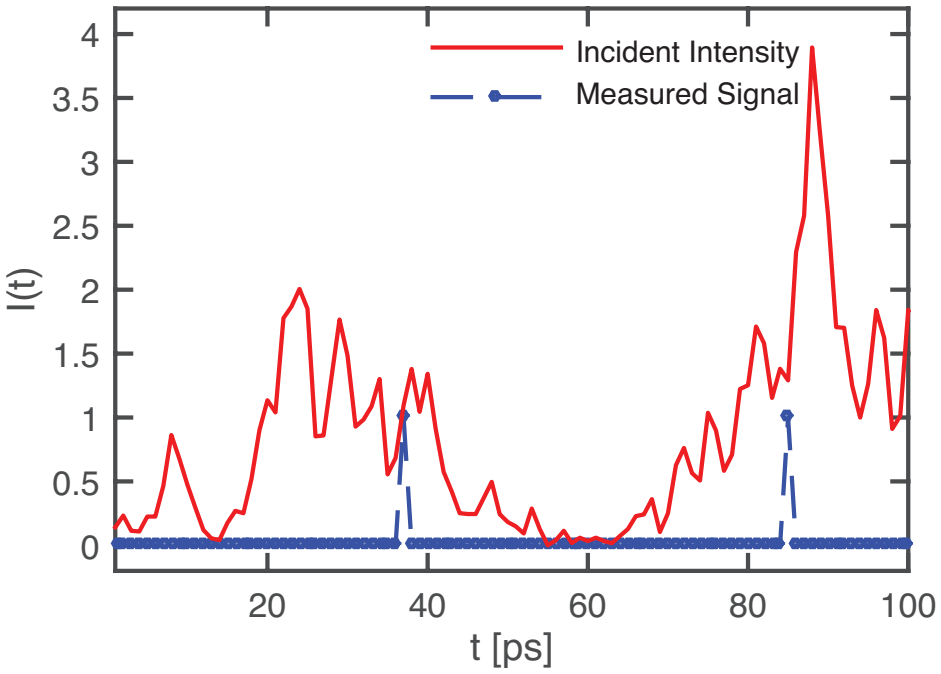

Figure 4.4: A time series from the random Gaussian signal that generates the data and the location of the discrete photoevents from the Poisson filter.

the future implementation of streak cameras, the determination of the complete shape of the autocorrelation function will be achievable. Also, the results typically obtained through XPCS analysis become possible using a simpler, less data-intensive histogram-based approach. Extending the time-scales accessible at synchrotron sources into the picosecond range would be a major advancement; many important physical and chemical processes [39, 40, 41, 42, 43, 44, 45, 46, 47, 48] take place in an intermediate regime that is much slower than FEL pulse durations (femtoseconds), but much faster than the synchrotron pulse spacing (nanoseconds).

This chapter is, in full, is a reprint of the material as it appears in: J. Wingert, A. Singer, and O.G. Shpyrko. A new method for studying sub-pulse dynamics at synchrotron

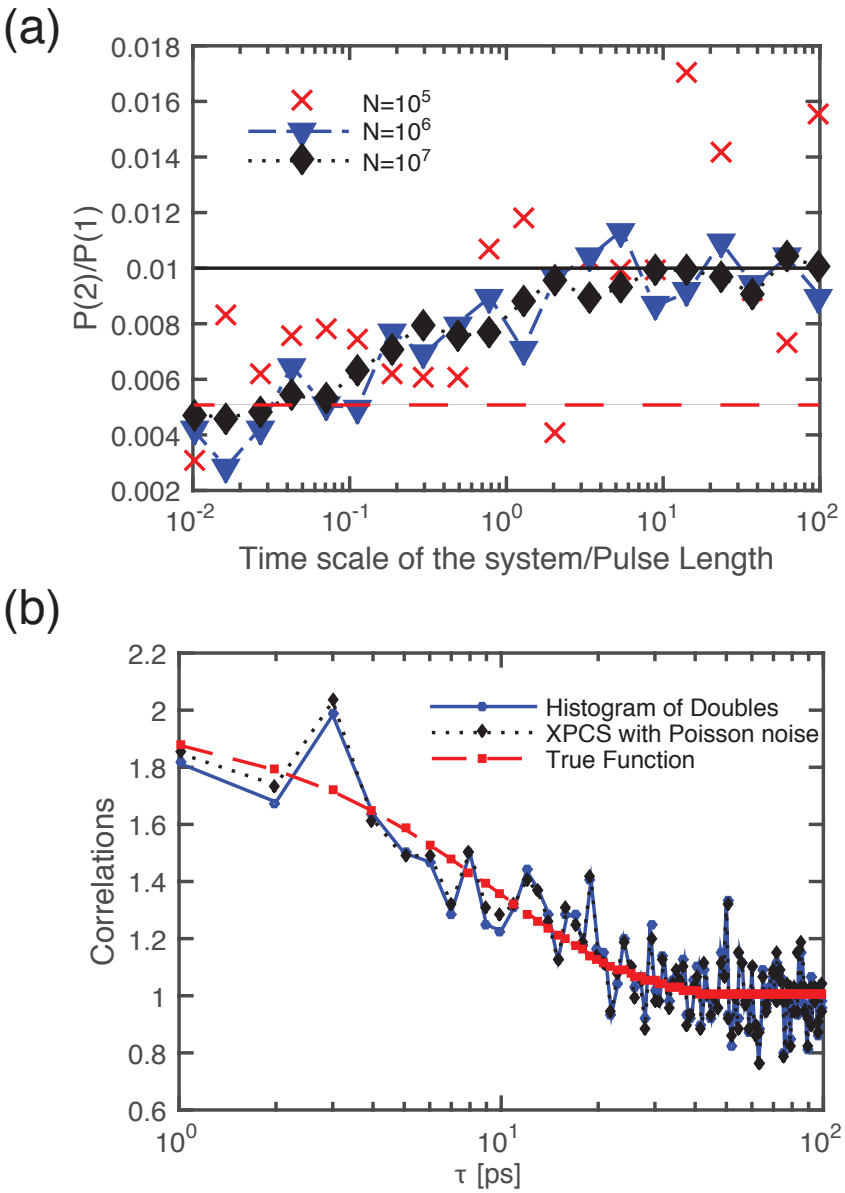

Figure 4.5: (a) The relative frequency of a double vs. the time-scale of the system, for different sample sizes. The horizontal lines represent the limiting quasi-static (solid black) and dynamic (dashed red) cases. (b) A normalized histogram of the number of doubles vs. the time separating them, plotted alongside g_2.

Table 4.1: Time required for a 3σ result for selected values of m

Source	photons/pixel/pulse, m	pixels required, N	time required
APS, "typical" experiment	$1.5\text{x}10^{-6}$	$8\text{x}10^{12}$	330 hrs (150 ns pulse spacing)
APS, partial direct beam	0.015	$9\text{x}10^{4}$	7 ms (150 ns pulse spacing)
APS upgrade, "typical" experiment	$7.5\text{x}10^{-5}$	$3.2\text{x}10^{9}$	4 min (75 ns pulse spacing)
APS upgrade, partial direct beam	0.19^{*}	1400	240 μs (75 ns pulse spacing)

m should actually be 0.75 in this approximation; the smaller value used corresponds to a minimum in N.

sources. Journal of Synchrotron Radiation 22, no. 5 (2015): 1141-1146.. The dissertation author was the primary investigator and author of this paper.

Chapter 5

Direct time-domain determination of electron-phonon coupling strengths in Chromium

We report the results of an ultrafast, direct structural measurement of optically pumped phonons in a Cr thin film using ultrashort x-ray pulses from a free-electron laser. In addition to measuring and confirming the known long-wavelength dispersion relation of Cr along a particular acoustic branch, we are able to determine the relative phase of the phonons as they are generated. Our sample exhibits two generation mechanisms for the phonons: the releasing of a pre-existing charge density wave at higher frequencies, and the creation of an acoustic strain pulse via laser heating that dominates at lower frequencies. For the later mechanism, we are able to measure the frequency dependence of the time required to generate the phonons. To explain the observed magnitude and slope

of the delays, we perform first principles simulations in the framework of perturbative density functional theory and ab initio molecular dynamics. These results show that the frequency dependence of the electron-phonon coupling is the driving mechanism behind the delay times, and that they have the correct slope with respect to frequency. However, the absolute magnitudes of the delay times measured are found to be much shorter than the equilibrium electron-phonon coupling times we compute, indicating that the coupling strength is greatly enhanced when the electronic system is out of equilibrium with the lattice.

Understanding the interactions between electrons and phonons in condensed matter systems is of both fundamental and practical importance. Until quite recently, the primary methods for studying phonons in solids have been inelastic scattering techniques. Inelastic neutron scattering (INS) has been used extensively for several decades to characterize the dispersion relations of a wide range of materials, including Chromium [49] [50]. More recently, frequency-domain studies using x-rays have also driven advances in our understanding of phonons in condensed matter systems. [51] Ultrafast electron diffraction has been employed to measure direct structural responses to optical excitation, but this has primarily been limited to studying the time evolution of the central Bragg peak [52][53] [54]. The direct time-domain measurement of structural changes in solids using x-rays on ultrafast ($< 1ps$) timescales has only become possible in the last several years. Although x-ray pump-probe techniques have been used for some time at synchrotron sources [55], it is the extremely short pulses ($< 50fs$) that can be generated by free-electron lasers (FELs) that have pushed these techniques into the ultrafast regime and allowed for the

direct detection of picosecond lattice oscillations [56] [57] [58] [59] [60] [61] [62]. It has been possible for some time to generate laser pulses of similarly short duration. For this reason, ultrafast pump-probe experiments using a laser pump and a laser probe were possible long before x-rays could be used as a probe to study the same timescales. It was these all-optical pump-probe studies that allowed for the determination of electron-phonon relaxation times in various materials, including Cr [63]. However, these studies, which typically measure ultrafast changes in reflectivity, are only sensitive to the rate of electron cooling. Measuring acoustic pulses propagate via reflectivity is also possible, but this approach effectively integrates the phonon response across all frequencies [64]. Now, with the ability to use ultrafast x-ray pulses to measure directly the phonons that are generated as the electronic system cools with a variety of specific wavevectors, it is possible to determine the rate at which phonons of different frequencies are generated, as in this study.

When an optical pulse is incident on a metal, it becomes absorbed primarily by the free electrons that lie within the optical penetration depth (about 20nm at a wavelength of 800nm in Cr). In our experiment, the laser pulse is incident on the sample at an angle of roughly 30° so that, normal to the film surface, the penetration depth is reduced to about 10nm. The hot electrons then diffuse further into the metal, during which time thermal diffusion also takes place. The depth to which these hot electrons can diffuse (about 15nm for Cr) is determined by the strength of electron-phonon coupling in the particular material [63]. Once the energy is transferred to the lattice, there is a displacement field and associated strain profile created over a distance that is determined by these two length scales (as well as a smaller contribution from thermal diffusion). If this distance is relatively

short (as it is in Cr), the central frequency of the resulting acoustic pulse will be relatively high. In bulk Cr, which demonstrates strong electron-phonon coupling, this is about 50 GHz, whereafter the amplitudes of the oscillations decline monotonically. In a thin film such as ours, with a thickness not significantly longer than these length scales, the shape of the acoustic pulse may be somewhat changed. However, our goal here is not to attempt to recreate the precise spatio-temporal shape of the acoustic pulse we generate, but rather to characterize the generation of the individual phonons that comprise it. It should be noted that there are other mechanisms by which optical light can drive acoustic oscillations in solids [65] [66], but our data clearly show this is a primary generation mechanism at work in our experiment.

In materials that exhibit charge density wave (CDW) order, such as our Cr film, there is another mechanism by which acoustic phonons are created. The band structure of Cr results in spin density wave electronic ordering of the free electrons with a period that is incommensurate with the lattice periodicity [67]. This results in a CDW whereby the equilibrium positions of the atoms are sinusoidally modulated. Essentially, this is a frozen phonon. When an optical pulse with sufficient energy is absorbed by the electrons, the electronic order is destroyed, and there is an abrupt shift in the potential energy environment of the atoms. This allows the frozen phonon to propagate. [60][68] Unlike the optical heating mechanism that drives phonons in all metals, there is zero lag for this generation mechanism, and the phonon begins to ring immediately after the electronic temperature rises. We show that, rather than complicating our analysis, this "CDW mechanism" of phonon generation provides a reference to which we can compare those

generated via the "thermal mechanism." It should be emphasized, for the reader comparing this work (at room temperature) with our prior study of the same sample at cryogenic temperatures [60], that because of the higher temperature, the CDW has a lower spatial frequency and reduced amplitude, which are shifted by an amount consistent with previous studies [67].

Our sample is a 28nm thick RF-sputtered Chromium thin film, annealed at 500°C. The crystal orientation of the film and MgO substrate are both [001], as determined by x-ray diffraction. At the Advanced Photon Source (APS), the diffraction pattern around the central [002] Bragg peak was recorded using a point detector [68]. The results of this measurement are shown in figure 5.1 in black. Due to the highly uniform thickness of the film, well-resolved Laue fringes with high intensity are clearly visible out to high-order. At the XPP station of the Linac Coherent Light Source (LCLS) [58], the diffraction from this sample was measured with a 2-D detector – the Cornell-SLAC hybrid Pixel Array Detector (CSPAD). Throughout the experiment, the detector and incident beam were held fixed, at an x-ray scattering angle of $2\theta = 60°$. By rotating the sample slightly, we were able to record images corresponding to different cuts through the fringes along the Bragg rod. Three such images are also shown in figure 5.1 alongside the synchrotron data. Due to the mosaic spread in the sample, several Laue fringes are visible simultaneously at a given sample angle[60]. All measurements were carried out at room temperature. It should be emphasized that the high intensity of the Laue fringes out to high order is what allows us to measure a strong signal in regions of momentum space that would typically exhibit only weak diffuse scattering.

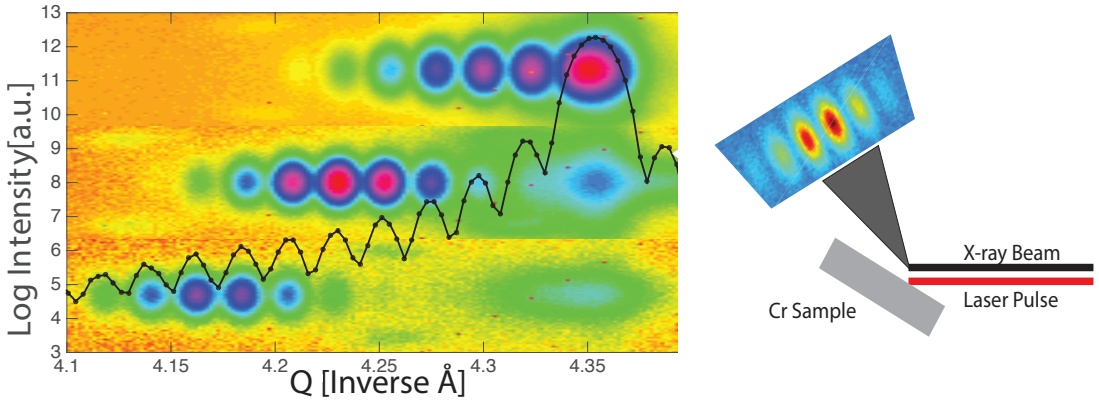

Figure 5.1: The axes and black data points are from data taken at APS. The central peak is the [002] Bragg peak for Cr, and the Laue fringes around it have a periodicity corresponding to the 28nm film thickness. Shown behind this are three separate area detector images taken at LCLS, corresponding to different cuts through these fringes on the Bragg rod, achieved by rocking the sample. On the right, a simple schematic of the experimental setup is shown.

For our pump-probe measurements, the sample was optically pumped with an 800 nm, 40 fs duration laser pulse. The energy delivered to the sample was about 5 mJ/cm^2, as determined using a reference sample. Diffraction patterns were then collected by probing the sample with a 15fs x-ray pulse (λ=0.14nm) at delay times ranging from -2ps to 10ps. This was done at several sample angles, so that, on the "low-Q" side relative to the Bragg peak, data was collected out to the 10th-order Laue fringe. The laser pump and x-ray probe had beam diameters of 0.5mm and 0.2mm, respectively. Conveniently, although the relative brightness of each fringe changes dramatically when the sample is rotated, the fringe positions on the detector move by less than a pixel. This allows us to combine multiple images directly, without making geometric corrections. After being summed, the combined images are then integrated vertically (with respect to the images in figure 5.1). This is done for the images collected at all possible delay times, so that we are left with

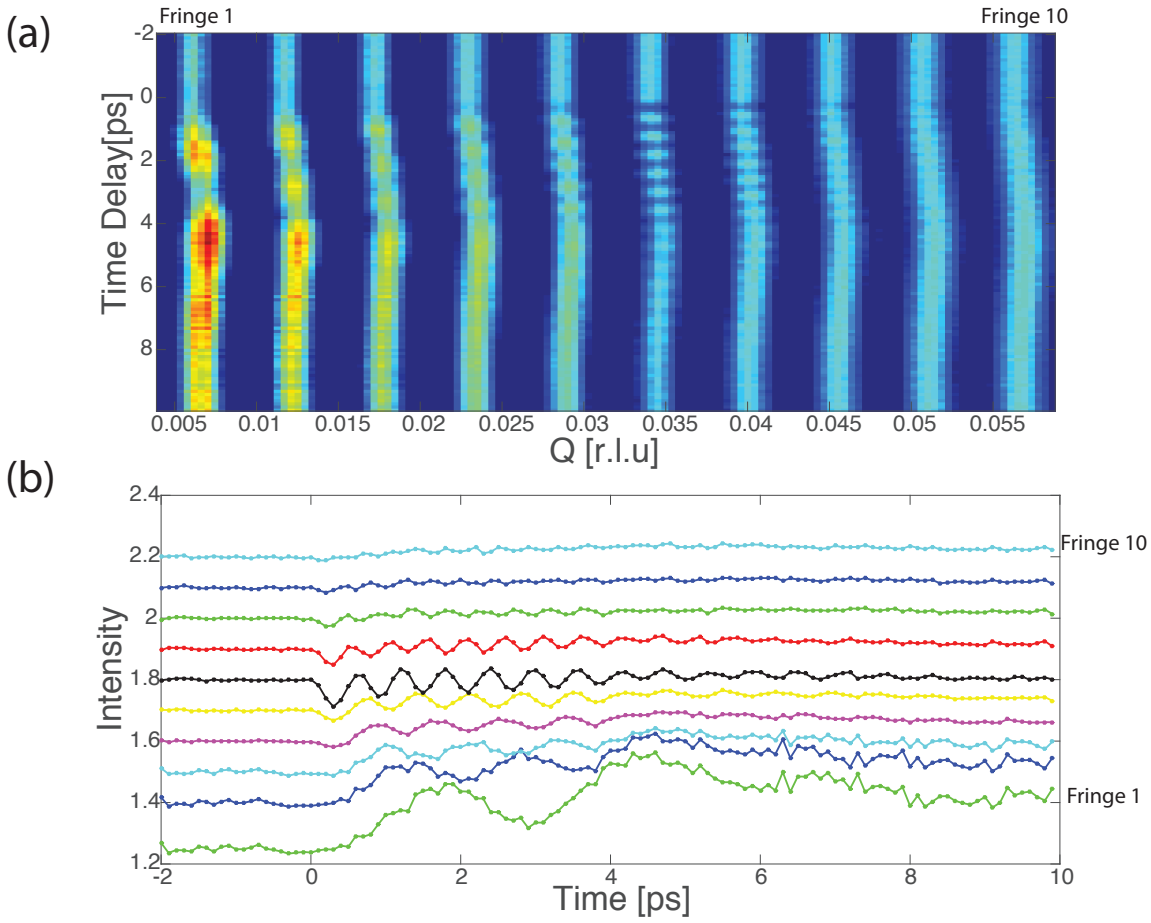

Figure 5.2: **(a)** All slices through the Bragg rod for the low-Q fringes combined in one image, integrated vertically with respect to figure 5.1, normalized by the $t < 0$ values, and plotted vs. time (Bragg peak not shown). **(b)** The extracted 1-D signals for the fringes shown in (a).

intensity values as a function of Q and time. In figure 5.2(a), a combined image of all measurements made on the low-Q side of the Bragg peak are shown. The intensities have been normalized by the $t < 0$ values to make the oscillations more clearly visible for all fringes.

To extract a simple one-dimensional intensity signal vs. time for the separate fringes, we identify for each of them a range of pixel values along Q that clearly do not

overlap with neighboring fringes, yet still fully contain the fringe as it shifts in Q slightly during the measurement (due to a slow oscillation of the central Bragg peak). These regions are then integrated over this small range of Q values, which results in a one-dimensional vector of intensities as a function of time delay. These resulting time series are shown in figure 5.2(b). After the signals are obtained for each fringe, we take their Fourier transforms in time. We then fit Gaussians to the main peaks identified in the amplitudes of the transforms. The means and standard deviations obtained from each of these fits serve as our frequency data points and error bars, respectively. These are plotted versus the Q value associated with each fringe (in units relative to Q_{Bragg}) in figure 5.3. A linear regression is performed to determine the slope of the best fit line for these points. Because we are in the long-wavelength limit where phonons propagate at a velocity $v = \omega/K$ [69], the slope of this line should give the speed of sound in our film, for longitudinal waves in the $< 001 >$ direction. This is found to be 7.45 nm/ps in our sample, which is in good agreement with data from inelastic neutron scattering [49]. The amplitudes of the Fourier transforms are also plotted in figure 5.3. The enhanced amplitude of the signal for fringe 6 and its neighbors is consistent with the existence of a residual charge-density wave with a periodicity centered on fringe 6, which persists above the Néel temperature for our thin film [60] [67]. A notable feature of the data is the reduced amplitude of the oscillations that occurs at about 4ps. This corresponds to the time it takes sound to propagate across the film at the velocity we observed, and confirms that we indeed generate an acoustic pulse at the free interface which then travels across the film, before being reflected by the MgO substrate.

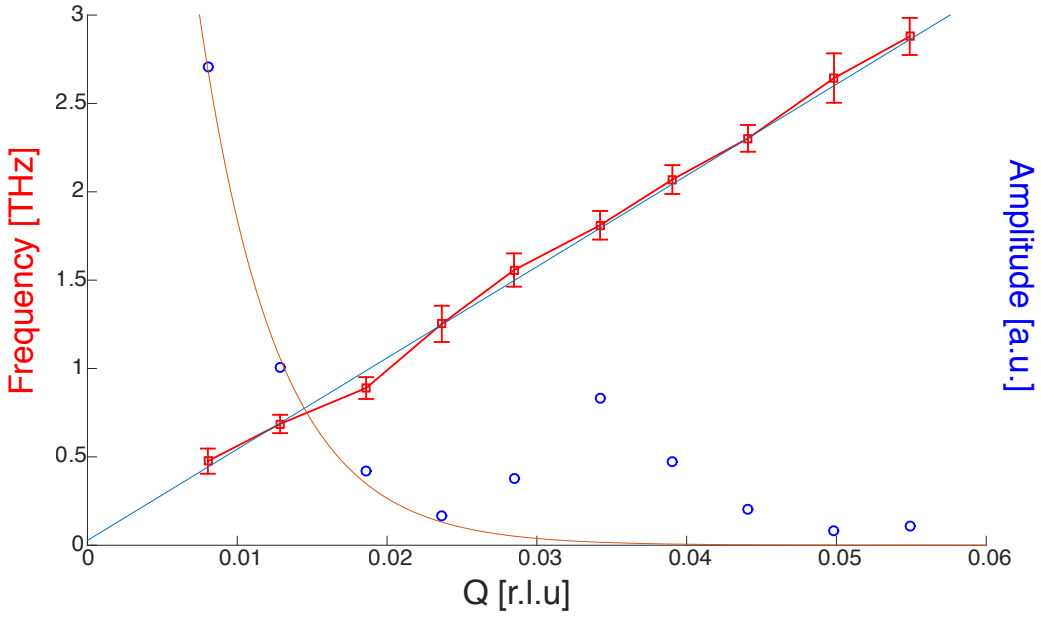

Figure 5.3: The dispersion curve points for all measured fringes on the low-Q side are shown, along with their amplitudes. The height of the Gaussians fitted to the Fourier transforms of the time signals give the amplitudes associated with each frequency. The red curve is an exponential fit to the first 3 points. The blue line shown is a best fit through all the frequency data points, whose slope gives the longitudinal speed of sound in the Cr film normal to the surface, which is found to be 7.45 nm/ps for our sample. The enhancement of the amplitude for fringe 6 and its neighbors is attributed to residual charge density wave ordering that persists above the Néel temperature.

Because we directly measure the phonon oscillations in the time-domain, we are sensitive to their phase. To calculate the relative phase for each phonon frequency measured, we calculate the locations in time of the first 2 maxima in the oscillations, using a smoothing filter. We then divide these times by the period of the signal, which is determined from the Fourier analysis previously discussed, and subtract off an appropriate integer multiple of 2π. As can be seen directly from the raw data in figure 5.2(b), the first three fringes have a qualitatively different phase relation than the other fringes. Moreover, one would expect the amplitudes of the signals to decrease monotonically in Q, as occurs in bulk Cr after about 50 GHz, a far lower frequency than any measured here. Instead, the amplitudes begin to rise again after the fourth fringe. We attribute these deviations from expected bulk behavior to the presence of two distinct phonon generation mechanisms. For the higher-order fringes, the response is driven by the presence of a CDW that begins to ring in our sample immediately after the electrons become hot. For the lowest order fringes, the generation mechanism is the typical heating/strain pulse mechanism. These phonons are only generated on the timescale of the electron-phonon relaxation time, which is known to be about 0.4 ps in Cr from reflectivity measurements [70]. For both mechanisms, if the proper effective $t = 0$ is identified, the response should be of a plus or minus cosine form. If this is accepted, then we can determine where the effective $t = 0$ must lie to give our signals this phase relation. In particular, we require that the first 3 fringes have a cosine response, and the others a minus cosine response, and then shift the effective $t = 0$ for each fringe to achieve this. The results are shown in figure 5.4(a). The higher order fringes (4-10) need little adjustment to achieve the ideal phase relation

we impose, because they are generated instantaneously upon laser heating, while the first three fringes demonstrate a lag time that is close to the known global electron-phonon relaxation time in Cr (It should be noted that for the higher order fringes, the periods and phase adjustments become smaller than the the experimental timing uncertainty, so they are of limited value). This lag time decreases with frequency, so that the longest wavelength phonons take the longest to populate. This turns out to be primarily due to the frequency dependence of electron-phonon interactions, as we will discuss. It may also be partly attributed to a speed of sound effect, owing to the fact that establishing a longer-wavelength collective mode requires communication between atoms at a longer distance, which presumably occurs at the speed of sound. There may also be some anharmonic phonon-phonon interactions driving the delay, but we show this effect is small.

To separate the processes involved in the ultrafast creation and dissipation of electronic and phononic states in Cr, we perform first principles simulations of the electron-phonon coupling. The structural and vibrational properties of Cr are well described by a spin-less DFT calculation (see SI for phonon band structures and spectral functions). We start by calculating the Éliashberg coupling constant λ, which integrates the coupling of all phonons with all electrons, and find $\lambda \simeq 0.1$ and $\lambda\langle\omega^2\rangle \simeq 66.49\,\mathrm{meV}^2$. The electron-phonon coupling (EPC) was previously extracted from experiment by Dresselhaus et al.[71], who find a moderate λ of 0.13 and $\lambda\langle\omega^2\rangle$ $\sim$128 meV^2. The difference may be due to our neglect of spin (see comments on Cr in Ref. [71]), or their use of a rough estimate for the average frequency, but in any event we have a fair representation of the global EPC.

The creation of phonons by a thermal (300 K) distribution of electrons can be char-

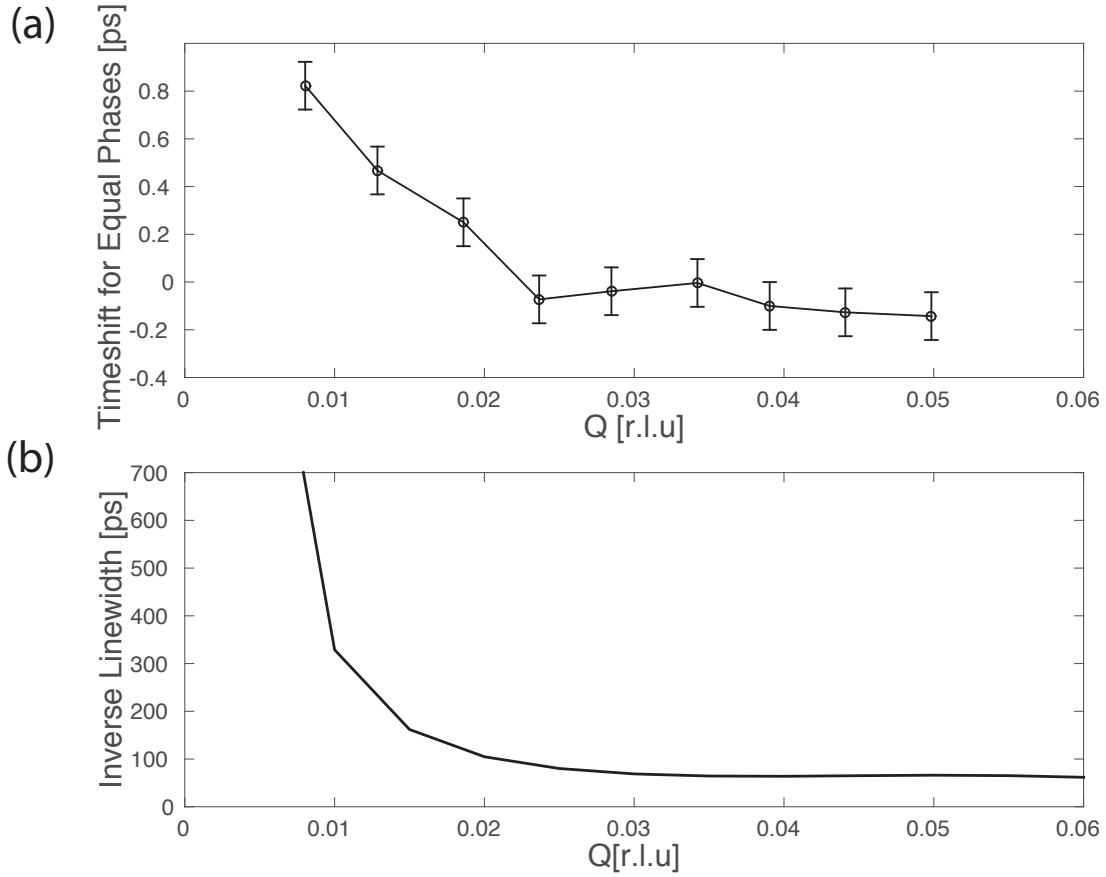

Figure 5.4: (a) Experimental phonon generation lag times: the time by which $t = 0$ must be shifted for each fringe to achieve the phase relation we expect. (b) Calculated acoustic phonon mode equilibrium lifetimes in Cr, for small $\vec{q}$ along the high symmetry $\Gamma - -H$ line.

acterized by the inverse of the EPC phonon line-width γ. These are plotted as a function of wave vector $\vec{q}$ in Fig. 5.4(b), with a dashed line delimiting the range corresponding to the experimental reflections for the thin film. There is a universal phase space restriction for small q phonon scattering: for small enough $\vec{q}$ the intersection of the phonon sphere with a given portion of the Fermi surface becomes a circle of decreasing diameter. This restricted phase space limits scattering and leads to the observed increase of the inverse line-width, which should vary as $1/q^2$ for small q. A fit to the ab initio data below 0.01 r.l.u. gives an exponent of -1.78.

The decrease with $\vec{q}$ is qualitatively similar to experiment, but the inverse line-widths are 2-3 orders of magnitude larger than the impulsive time delays measured in experiment. This reflects the equilibrium statistical nature of the line-widths, and the crucial difference with the decay of a non-equilibrium distribution of electrons. Zone edge equilibrium line-widths are much larger, corresponding to lifetimes down to 4-5 ps. The coupling time estimated from figure 1 in Dresselhaus et al. cumulates electrons scattering out into all phonon modes (mainly large $\vec{q}$ to access the whole Fermi Surface). For small $\vec{q}$ phonons, the response time are dominated by the impulsive non-equilibrium effects, but follow the same "phase space" dependency on $\vec{q}$.

In order to discard that the observed response is not driven by phonon-phonon interactions, we have performed a calculation of the phonon-phonon linewidth by ab initio molecular dynamics and mapping the interatomic force constants to any order by using the TDEP method as developed in Ref. [72]. Our calculations clearly show that the phonon-phonon line-widths are at least one order of magnitude smaller than the electron-phonon,

which implies that we can safely discard the phonon-phonon contribution and that the observed process is led by the electron-phonon coupling.

To describe the electron-phonon interaction, we employ the ABINIT software package [73], which implements DFT and DFPT. We use the norm conserving pseudopotential framework (using the ONCVPSP scheme of Hamann[74]) and a plane wave basis set up to kinetic energies of 40 Ha. We have also used the Local Density Approximation (LDA) to describe the exchange correlation functional and we also use the experimental value of the cell parameter. Phonons and EPC are calculated within the density functional perturbation theory[75, 76].

On the other hand, the phonon-phonon TDEP calculations were extracted from ab-initio molecular dynamics calculations using the VASP code [77, 78]. This code relies on the PAW representation for the wave function with an energy cutoff of 500eV, and the same energy functional used in the ABINIT calculation.

In summary, we have demonstrated the generation of phonons in Cr via ultrafast optical excitation attributed to two distinct generation mechanisms – the releasing of a frozen CDW, and the generation of a coherent acoustic strain pulse. The CDW phonons have a response that is instantaneous upon heating of the electronic system, whereas those associated with the acoustic pulse demonstrate a generation lag and a dependence on the phonon frequency. Through phase-space considerations and PDFT calculations, we show that this frequency dependence is driven by the variable electron-phonon coupling strength, and has the correct slope, but is three orders of magnitude faster than predicted by the equilibrium calculations. This points to a greatly enhanced scattering rate when the hot

electrons are out of equilibrium with the lattice. This might be explored experimentally by varying the laser fluence and observing the effect on the phonon generation times. Theoretically, a non-equilibrium description of the system may be able to explain the observed electron-phonon coupling magnitudes in the future.

The work at UCSD was supported by U.S. Department of Energy, Office of Science, Office of Basic Energy Sciences,under Contracts No. DE-SC0001805 (ultrafast x-ray scattering, A. S., R. K., J. W., and O. G. S.) and No. DESC0003678 (thin films synthesis and characterization, S. K. K. P., R. K., V. U., and E. E. F.). O. M. M., B. M. M., and S. F. thank the Bundesministerium für Bildung und Forschung (BMBF) for financial support via Project No. 05K13FK2. Use of the Linac Coherent Light Source (LCLS), SLAC National Accelerator Laboratory, is supported by the U.S. Department of Energy, Office of Science, Office of Basic Energy Sciences under Contract No. DEAC02-76SF00515. This research used resources of the Advanced Photon Source (APS), a U.S. Department of Energy (DOE) Office of Science User Facility operated for the DOE Office of Science by Argonne National Laboratory under Contract No. DE-AC02-06CH11357. We would like to acknowledge the support we received from Alec Sandy and Eric Dufresne of APS.

This chapter is, in full, is a reprint of a draft in preparation for submission: J. Wingert, A. Singer, S. K. K. Patel, R. Kukreja, M. Verstraete, A. Romero, V. Uhlíř, S. Festersen, D. Zhu, J. M. Glownia, H. T. Lemke, S. Nelson, M. Kozina, K. Rossnagel, B. M. Murphy, O. M. Magnussen, E. E. Fullerton, and O. G. Shpyrko Direct time-domain determination of electron-phonon coupling strengths in Chromium. (To be submitted, working title.) The dissertation author was the primary investigator and author of this

paper.

Bibliography

[1] J. Als-Nielsen and D. McMorrow, *Elements of modern X-ray physics*. John Wiley & Sons, 2011.

[2] B. D. Cullity and J. W. Weymouth, "Elements of x-ray diffraction," *American Journal of Physics*, vol. 25, no. 6, pp. 394–395, 1957.

[3] B. E. Warren, *X-ray Diffraction*. Courier Corporation, 1969.

[4] B. J. Berne and R. Pecora, *Dynamic light scattering: with applications to chemistry, biology, and physics*. Courier Dover Publications, 2000.

[5] J. W. Goodman, *Speckle phenomena in optics: theory and applications*. Roberts and Company Publishers, 2007.

[6] W. Goldburg, "Dynamic light scattering," *American Journal of Physics*, vol. 67, no. 12, pp. 1152–1160, 1999.

[7] Y. Chou and W. I. Goldburg, "Angular distribution of light scattered from critically quenched liquid mixtures," *Physical Review A*, vol. 23, no. 2, p. 858, 1981.

[8] P. Debye and K. Kleboth, "Electrical field effect on the critical opalescence," *The Journal of Chemical Physics*, vol. 42, no. 9, pp. 3155–3162, 1965.

[9] E. M. Dufresne, T. Nurushev, R. Clarke, and S. B. Dierker, "Concentration fluctuations in the binary mixture hexane-nitrobenzene with static and dynamic x-ray scattering," *Physical Review E*, vol. 65, no. 6, p. 061507, 2002.

[10] P. Falus, M. Borthwick, S. Narayanan, A. Sandy, and S. Mochrie, "Crossover from stretched to compressed exponential relaxations in a polymer-based sponge phase," *Physical review letters*, vol. 97, no. 6, p. 066102, 2006.

[11] L. Cipelletti, L. Ramos, S. Manley, E. Pitard, D. A. Weitz, E. E. Pashkovski, and M. Johansson, "Universal non-diffusive slow dynamics in aging soft matter," *Faraday Discussions*, vol. 123, pp. 237–251, 2003.

[12] R. Bandyopadhyay, A. Gittings, S. Suh, P. Dixon, and D. Durian, "Speckle-visibility spectroscopy: A tool to study time-varying dynamics," *Review of scientific instruments*, vol. 76, no. 9, p. 093110, 2005.

[13] I. Inoue, Y. Shinohara, A. Watanabe, and Y. Amemiya, "Effect of shot noise on x-ray speckle visibility spectroscopy," *Optics express*, vol. 20, no. 24, pp. 26878–26887, 2012.

[14] C. Gutt, L.-M. Stadler, A. Duri, T. Autenrieth, O. Leupold, Y. Chushkin, and G. Grübel, "Measuring temporal speckle correlations at ultrafast x-ray sources," *Optics express*, vol. 17, no. 1, pp. 55–61, 2009.

[15] J. Carnis, W. Cha, J. Wingert, J. Kang, Z. Jiang, S. Song, M. Sikorski, A. Robert, C. Gutt, S.-W. Chen, *et al.*, "Demonstration of feasibility of x-ray free electron laser studies of dynamics of nanoparticles in entangled polymer melts," *Scientific reports*, vol. 4, 2014.

[16] C. Bressler, C. Milne, V.-T. Pham, A. Elnahhas, R. M. van der Veen, W. Gawelda, S. Johnson, P. Beaud, D. Grolimund, M. Kaiser, C. N. Borca, G. Ingold, R. Abela, and M. Chergui, "Femtosecond XANES study of the light-induced spin crossover dynamics in an iron(II) complex.," *Science (New York, N.Y.)*, vol. 323, pp. 489–92, Jan. 2009.

[17] M. Trigo, M. Fuchs, J. Chen, M. P. Jiang, M. Cammarata, S. Fahy, D. M. Fritz, K. Gaffney, S. Ghimire, A. Higginbotham, S. L. Johnson, M. E. Kozina, J. Larsson, H. Lemke, A. M. Lindenberg, G. Ndabashimiye, F. Quirin, K. Sokolowski-Tinten, C. Uher, G. Wang, J. S. Wark, D. Zhu, and D. A. Reis, "Fourier-transform inelastic X-ray scattering from time- and momentum-dependent phononphonon correlations," *Nature Physics*, vol. 9, pp. 790–794, Oct. 2013.

[18] L. Young, E. Kanter, B. Krässig, Y. Li, A. March, S. Pratt, R. Santra, S. Southworth, N. Rohringer, L. DiMauro, *et al.*, "Femtosecond electronic response of atoms to ultra-intense x-rays," *Nature*, vol. 466, no. 7302, pp. 56–61, 2010.

[19] E. Möhr-Vorobeva, S. L. Johnson, P. Beaud, U. Staub, R. De Souza, C. Milne, G. Ingold, J. Demsar, H. Schaefer, and A. Titov, "Nonthermal melting of a charge density wave in tise 2," *Physical review letters*, vol. 107, no. 3, p. 036403, 2011.

[20] W. a. Ackermann, G. Asova, V. Ayvazyan, A. Azima, N. Baboi, J. Bähr, V. Balandin, B. Beutner, A. Brandt, A. Bolzmann, *et al.*, "Operation of a free-electron laser from the extreme ultraviolet to the water window," *Nature photonics*, vol. 1, no. 6, pp. 336–342, 2007.

[21] P. Emma, R. Akre, J. Arthur, R. Bionta, C. Bostedt, J. Bozek, A. Brachmann, P. Bucksbaum, R. Coffee, F. J. Decker, Y. Ding, D. Dowell, S. Edstrom, A. Fisher, J. Frisch, S. Gilevich, J. Hastings, G. Hays, HeringPh., Z. Huang, R. Iverson, H. Loos, M. Messerschmidt, A. Miahnahri, S. Moeller, H. D. Nuhn, G. Pile, D. Ratner,

J. Rzepiela, D. Schultz, T. Smith, P. Stefan, H. Tompkins, J. Turner, J. Welch, W. White, J. Wu, G. Yocky, and J. Galayda, "First lasing and operation of an angstrom-wavelength free-electron laser," *Nat Photon*, vol. 4, pp. 641–647, Sept. 2010.

[22] T. Ishikawa, H. Aoyagi, T. Asaka, Y. Asano, N. Azumi, T. Bizen, H. Ego, K. Fukami, T. Fukui, Y. Furukawa, *et al.*, "A compact x-ray free-electron laser emitting in the sub-angstrom region," *nature photonics*, vol. 6, no. 8, pp. 540–544, 2012.

[23] E. Allaria, R. Appio, L. Badano, W. Barletta, S. Bassanese, S. Biedron, A. Borga, E. Busetto, D. Castronovo, P. Cinquegrana, *et al.*, "Highly coherent and stable pulses from the fermi seeded free-electron laser in the extreme ultraviolet," *Nature Photonics*, vol. 6, no. 10, pp. 699–704, 2012.

[24] M. Sutton, S. G. J. Mochrie, T. Greytak, S. E. Nagler, L. E. Berman, G. A. Held, and G. B. Stephenson, "Observation of speckle by diffraction with coherent X-rays," *Nature*, vol. 352, pp. 608–610, Aug. 1991.

[25] G. Grübel and F. Zontone, "Correlation spectroscopy with coherent X-rays," *Journal of Alloys and Compounds*, vol. 362, no. 1–2, pp. 3–11, 2004.

[26] O. Shpyrko, E. Isaacs, J. Logan, Y. Feng, G. Aeppli, R. Jaramillo, H. Kim, T. Rosenbaum, P. Zschack, M. Sprung, *et al.*, "Direct measurement of antiferromagnetic domain fluctuations," *Nature*, vol. 447, no. 7140, pp. 68–71, 2007.

[27] I. Sikharulidze, B. Farago, I. P. Dolbnya, A. Madsen, and W. H. de Jeu, "Surface and bulk elasticity determined fluctuation regimes in smectic membranes," *Physical review letters*, vol. 91, no. 16, p. 165504, 2003.

[28] R. H. Brown and R. Twiss, "Correlation between photons in two coherent beams of light," *Nature*, vol. 177, no. 4497, pp. 27–29, 1956.

[29] E. Ikonen, "Interference effects between independent gamma rays," *Physical review letters*, vol. 68, no. 18, p. 2759, 1992.

[30] S. Kishimoto, N. Ishizawa, and T. Vaalsta, "A fast detector using stacked avalanche photodiodes for x-ray diffraction experiments with synchrotron radiation," *Review of scientific instruments*, vol. 69, no. 2, pp. 384–391, 1998.

[31] K. Namikawa, M. Kishimoto, K. Nasu, E. Matsushita, R. Tai, K. Sukegawa, H. Yamatani, H. Hasegawa, M. Nishikino, M. Tanaka, and K. Nagashima, "Direct Observation of the Critical Relaxation of Polarization Clusters in BaTiO3 Using a Pulsed X-Ray Laser Technique," *Physical Review Letters*, vol. 103, p. 197401, Nov. 2009.

[32] J. Itatani, F. Quéré, G. Yudin, M. Ivanov, F. Krausz, and P. Corkum, "Attosecond Streak Camera," *Physical Review Letters*, vol. 88, p. 173903, Apr. 2002.

[33] Z. Chang, A. Rundquist, J. Zhou, M. M. Murnane, H. C. Kapteyn, X. Liu, B. Shan, J. Liu, L. Niu, M. Gong, and X. Zhang, "Demonstration of a sub-picosecond x-ray streak camera," *Applied Physics Letters*, vol. 69, p. 133, July 1996.

[34] S. Hruszkewycz, M. Sutton, P. Fuoss, B. Adams, S. Rosenkranz, K. Ludwig Jr, W. Roseker, D. Fritz, M. Cammarata, D. Zhu, *et al.*, "High contrast x-ray speckle from atomic-scale order in liquids and glasses," *Physical review letters*, vol. 109, no. 18, p. 185502, 2012.

[35] S. M. Ross, *Introduction to probability models*. Academic press, 2006.

[36] P. Falus, L. B. Lurio, and S. G. J. Mochrie, "Optimizing the signal-to-noise ratio for X-ray photon correlation spectroscopy.," *Journal of synchrotron radiation*, vol. 13, pp. 253–9, May 2006.

[37] A. Singer and I. A. Vartanyants, "Modelling of partially coherent radiation based on the coherent mode decomposition," in *SPIE Optical Engineering+ Applications*, pp. 814106–814106, International Society for Optics and Photonics, 2011.

[38] T. Pfeifer, Y. Jiang, S. Düsterer, R. Moshammer, and J. Ullrich, "Partial-coherence method to model experimental free-electron laser pulse statistics," *Opt. Lett.*, vol. 35, pp. 3441–3443, Oct. 2010.

[39] A. Vaterlaus, T. Beutler, and F. Meier, "Spin-lattice relaxation time of ferromagnetic gadolinium determined with time-resolved spin-polarized photoemission," *Physical review letters*, vol. 67, no. 23, p. 3314, 1991.

[40] P. V. Kamat, M. Flumiani, and G. V. Hartland, "Picosecond dynamics of silver nanoclusters. photoejection of electrons and fragmentation," *The Journal of Physical Chemistry B*, vol. 102, no. 17, pp. 3123–3128, 1998.

[41] A. Harris, J. Brown, and C. Harris, "The nature of simple photodissociation reactions in liquids on ultrafast time scales," *Annual Review of Physical Chemistry*, vol. 39, no. 1, pp. 341–366, 1988.

[42] E. Beaurepaire, J.-C. Merle, A. Daunois, and J.-Y. Bigot, "Ultrafast spin dynamics in ferromagnetic nickel," *Physical Review Letters*, vol. 76, no. 22, p. 4250, 1996.

[43] A. Scholl, L. Baumgarten, R. Jacquemin, and W. Eberhardt, "Ultrafast spin dynamics of ferromagnetic thin films observed by fs spin-resolved two-photon photoemission," *Physical review letters*, vol. 79, no. 25, p. 5146, 1997.

[44] F. Raksi, K. R. Wilson, Z. Jiang, A. Ikhlef, C. Y. Côté, and J.-C. Kieffer, "Ultrafast x-ray absorption probing of a chemical reaction," *The Journal of chemical physics*, vol. 104, no. 15, pp. 6066–6069, 1996.

[45] C. Shank, R. Yen, R. Fork, J. Orenstein, and G. Baker, "Picosecond dynamics of photoexcited gap states in polyacetylene," *Physical Review Letters*, vol. 49, no. 22, p. 1660, 1982.

[46] J. A. McCammon, P. G. Wolynes, and M. Karplus, "Picosecond dynamics of tyrosine side chains in proteins," *Biochemistry*, vol. 18, no. 6, pp. 927–942, 1979.

[47] A. Cavalleri, C. Tóth, C. W. Siders, J. Squier, F. Ráksi, P. Forget, and J. Kieffer, "Femtosecond structural dynamics in vo 2 during an ultrafast solid-solid phase transition," *Physical review letters*, vol. 87, no. 23, p. 237401, 2001.

[48] N. Serpone, D. Lawless, R. Khairutdinov, and E. Pelizzetti, "Subnanosecond relaxation dynamics in tio2 colloidal sols (particle sizes rp= 1.0-13.4 nm). relevance to heterogeneous photocatalysis," *The Journal of Physical Chemistry*, vol. 99, no. 45, pp. 16655–16661, 1995.

[49] W. Shaw and L. Muhlestein, "Investigation of the phonon dispersion relations of chromium by inelastic neutron scattering," *Physical Review B*, vol. 4, no. 3, p. 969, 1971.

[50] M. F. DeCamp, D. A. Reis, D. M. Fritz, P. H. Bucksbaum, E. M. Dufresne, and R. Clarke, "X-ray synchrotron studies of ultrafast crystalline dynamics," *Journal of synchrotron radiation*, vol. 12, no. 2, pp. 177–192, 2005.

[51] B. Murphy, H. Requardt, J. Stettner, J. Serrano, M. Krisch, M. Müller, and W. Press, "Phonon modes at the 2 h- nbse 2 surface observed by grazing incidence inelastic x-ray scattering," *Physical review letters*, vol. 95, no. 25, p. 256104, 2005.

[52] H. Park, X. Wang, S. Nie, R. Clinite, and J. Cao, "Mechanism of coherent acoustic phonon generation under nonequilibrium conditions," *Physical Review B*, vol. 72, no. 10, p. 100301, 2005.

[53] S. Nie, X. Wang, H. Park, R. Clinite, and J. Cao, "Measurement of the electronic grüneisen constant using femtosecond electron diffraction," *Physical review letters*, vol. 96, no. 2, p. 025901, 2006.

[54] T. Chase, M. Trigo, A. Reid, R. Li, T. Vecchione, X. Shen, S. Weathersby, R. Coffee, N. Hartmann, D. Reis, *et al.*, "Ultrafast electron diffraction from non-equilibrium phonons in femtosecond laser heated au films," *Applied Physics Letters*, vol. 108, no. 4, p. 041909, 2016.

[55] D. A. Reis and A. M. Lindenberg, "Ultrafast x-ray scattering in solids," in *Light Scattering in Solid IX*, pp. 371–422, Springer, 2006.

[56] M. Trigo, J. Chen, V. Vishwanath, Y. Sheu, T. Graber, R. Henning, and D. Reis, "Imaging nonequilibrium atomic vibrations with x-ray diffuse scattering," *Physical Review B*, vol. 82, no. 23, p. 235205, 2010.

[57] D. Zhu, A. Robert, T. Henighan, H. T. Lemke, M. Chollet, J. M. Glownia, D. A. Reis, and M. Trigo, "Phonon spectroscopy with sub-mev resolution by femtosecond x-ray diffuse scattering," *Physical Review B*, vol. 92, no. 5, p. 054303, 2015.

[58] M. Chollet, R. Alonso-Mori, M. Cammarata, D. Damiani, J. Defever, J. T. Delor, Y. Feng, J. M. Glownia, J. B. Langton, S. Nelson, *et al.*, "The x-ray pump–probe instrument at the linac coherent light source," *Journal of Synchrotron Radiation*, vol. 22, no. 3, pp. 503–507, 2015.

[59] M. Trigo, M. Fuchs, J. Chen, M. Jiang, M. Cammarata, S. Fahy, D. Fritz, K. Gaffney, S. Ghimire, A. Higginbotham, *et al.*, "Fourier-transform inelastic x-ray scattering from time-and momentum-dependent phonon-phonon correlations," *Nature Physics*, vol. 9, no. 12, pp. 790–794, 2013.

[60] A. Singer, S. Patel, R. Kukreja, V. Uhlíř, J. Wingert, S. Festersen, D. Zhu, J. Glownia, H. Lemke, S. Nelson, *et al.*, "Photoinduced enhancement of the charge density wave amplitude," *Physical Review Letters*, vol. 117, no. 5, p. 056401, 2016.

[61] K. Gaffney and H. Chapman, "Imaging atomic structure and dynamics with ultrafast x-ray scattering," *Science*, vol. 316, no. 5830, pp. 1444–1448, 2007.

[62] T. Henighan, M. Trigo, S. Bonetti, P. Granitzka, D. Higley, Z. Chen, M. Jiang, R. Kukreja, A. Gray, A. Reid, *et al.*, "Generation mechanism of terahertz coherent acoustic phonons in fe," *Physical Review B*, vol. 93, no. 22, p. 220301, 2016.

[63] T. Saito, O. Matsuda, and O. Wright, "Picosecond acoustic phonon pulse generation in nickel and chromium," *Physical Review B*, vol. 67, no. 20, p. 205421, 2003.

[64] C. Thomsen, H. T. Grahn, H. J. Maris, and J. Tauc, "Surface generation and detection of phonons by picosecond light pulses," *Physical Review B*, vol. 34, no. 6, p. 4129, 1986.

[65] H. Zeiger, J. Vidal, T. Cheng, E. Ippen, G. Dresselhaus, and M. Dresselhaus, "Theory for displacive excitation of coherent phonons," *Physical Review B*, vol. 45, no. 2, p. 768, 1992.

[66] K. Ishioka and O. V. Misochko, "Coherent lattice oscillations in solids and their optical control," in *Progress in Ultrafast Intense Laser Science*, pp. 23–46, Springer, 2010.

[67] E. Fawcett, "Spin-density-wave antiferromagnetism in chromium," *Reviews of Modern Physics*, vol. 60, no. 1, p. 209, 1988.

[68] A. Singer, M. Marsh, S. Dietze, V. Uhlíř, Y. Li, D. Walko, E. Dufresne, G. Srajer, M. Cosgriff, P. Evans, *et al.*, "Condensation of collective charge ordering in chromium," *Physical Review B*, vol. 91, no. 11, p. 115134, 2015.

[69] C. Kittel, *Introduction to solid state physics*. Wiley, 2005.

[70] S. Brorson, A. Kazeroonian, J. Moodera, D. Face, T. Cheng, E. Ippen, M. Dresselhaus, and G. Dresselhaus, "Femtosecond room-temperature measurement of the electron-phonon coupling constant γ in metallic superconductors," *Physical Review Letters*, vol. 64, no. 18, p. 2172, 1990.

[71] S. D. Brorson, A. Kazeroonian, J. S. Moodera, D. W. Face, T. K. Cheng, E. P. Ippen, M. S. Dresselhaus, and G. Dresselhaus, "Femtosecond room-temperature measurement of the electron-phonon coupling constant γ in metallic superconductors," *Phys. Rev. Lett.*, vol. 64, pp. 2172–2175, Apr 1990.

[72] O. Hellman, P. Steneteg, I. A. Abrikosov, and S. I. Simak, "Temperature dependent effective potential method for accurate free energy calculations of solids," *Physical Review B*, vol. 87, no. 10, p. 104111, 2013.

[73] X. Gonze, F. Jollet, F. A. Araujo, D. Adams, B. Amadon, T. Applencourt, C. Audouze, J.-M. Beuken, J. Bieder, A. Bokhanchuk, E. Bousquet, F. Bruneval, D. Caliste, M. Côté, F. Dahm, F. Da Pieve, M. Delaveau, M. Di Gennaro, B. Dorado, C. Espejo, G. Geneste, L. Genovese, A. Gerossier, M. Giantomassi, Y. Gillet, D. R. Hamann, L. He, G. Jomard, J. Laflamme Janssen, S. L. Roux, A. Levitt, A. Lherbier, F. Liu, Lukacevic, A. Martin, C. Martins, M. J. T. Oliveira, S. Ponce, Y. Pouillon, T. Rangel, G. Rignanese, A. H. Romero, B. Rousseau, O. Rubel, A. A. Shukri, M. Stankovski, M. Torrent, M. J. van Setten, B. Van Troeye, M. J. Verstraete, D. Waroquier, J. Wiktor, B. Xu, A. Zhou, and J. W. Zwanziger, "Recent developments in the abinit software package," *Comput. Phys. Commun.*, vol. 205, pp. 106–131, 2016.

[74] D. R. Hamann, "Optimized norm-conserving vanderbilt pseudopotentials," *Phys. Rev. B*, vol. 88, p. 085117, Aug 2013.

[75] S. Y. Savrasov and D. Y. Savrasov, "Electron-phonon interactions and related physical properties of metals from linear-response theory," *Phys. Rev. B*, vol. 54, pp. 16487–16501, Dec 1996.

[76] M. Verstraete and Z. Zanolli, "Density functional perturbation theory," in *Computing Solids: Models, Ab-initio Methods and Supercomputing, Lecture Notes of the 45th Spring School 2014* (S. Blügel, N. Helbig, V. Meden, and D. Wortmann, eds.), vol. 35 of *Schlüsseltechnologien Key Technologies*, (Jülich), pp. C2.1 – C2.29, Forschungszentrum Jülich, Schriften des Forschungszentrums Jülich, 2014.

[77] G. Kresse and J. Furthmüller, "Efficient iterative schemes for ab initio total-energy calculations using a plane-wave basis set," *Phys. Rev. B*, vol. 54, pp. 11169–11186, Oct 1996.

[78] G. Kresse and D. Joubert, "From ultrasoft pseudopotentials to the projector augmented-wave method," *Phys. Rev. B*, vol. 59, pp. 1758–1775, Jan 1999.